NASA TECHNICAL NOTE

NASA TN D-5742

NASA TN D-5742

LARGE-SCALE WIND-TUNNEL TESTS OF AN AIRPLANE MODEL WITH FOUR PROPELLERS AND ROTATING CYLINDER FLAPS

by James A. Weiberg and Stanley O. Dickinson

Ames Research Center
Moffett Field, Calif.

NATIONAL AERONAUTICS AND SPACE ADMINISTRATION • WASHINGTON, D. C. • APRIL 1970

1. Report No. NASA TN D-5742	2. Government Accession No.	3. Recipient's Catalog No.
4. Title and Subtitle LARGE-SCALE WIND-TUNNEL TESTS OF AN AIRPLANE MODEL WITH FOUR PROPELLERS AND ROTATING CYLINDER FLAPS		5. Report Date April 1970 6. Performing Organization Code
7. Author(s) James A. Weiberg and Stanley O. Dickinson		8. Performing Organization Report No. A-2769
9. Performing Organization Name and Address NASA Ames Research Center Moffett Field, Calif., 94035		10. Work Unit No. 721-01-00-13-00-21 11. Contract or Grant No.
12. Sponsoring Agency Name and Address National Aeronautics and Space Administration Washington, D.C. 20546		13. Type of Report and Period Covered Technical Note 14. Sponsoring Agency Code

15. Supplementary Notes

16. Abstract

Wind-tunnel tests were made of a model equipped with rotating cylindrical flaps and four propellers. Comparison with the results obtained with the same flap on a model with two propellers of larger diameter but with approximately the same slipstream coverage on the wing showed that large gains were obtained in the lift due to thrust and slipstream turning as a result of the increased flap chord relative to propeller diameter. The slipstream turning angles for the four-propeller model were approximately equal to the flap deflection.

17. Key Words Suggested by Author(s) Rotating cylinder flaps	18. Distribution Statement Unclassified - Unlimited		
19. Security Classif. (of this report) Unclassified	20. Security Classif. (of this page) Unclassified	21. No. of Pages 71	22. Price* $3.00

*For sale by the Clearinghouse for Federal Scientific and Technical Information
Springfield, Virginia 22151

NOTATION

b wing span, 26.17 ft

BLC boundary-layer control

C_D drag coefficient, $\frac{\text{drag}}{qS}$

C_{h_f} flap hinge-moment coefficient, $\frac{HM}{qS_f c_f}$

C_L lift coefficient, $\frac{\text{lift}}{qS}$

C_{L_α} lift-curve slope, $\frac{\partial C_L}{\partial \alpha}$

C_{L_δ} lift due to flap deflection, $\frac{\partial C_L}{\partial \delta_f}$

C_m pitching-moment coefficient, $\frac{M}{qSc}$

C_p power coefficient, $\frac{P}{\rho n^3 D^5}$

C_T thrust coefficient, $\frac{T}{\rho n^2 D^4}$

C_Y side-force coefficient, $\frac{Y}{qS}$

c wing chord, 4.89 ft

c_f flap chord aft of cylinder center line, 2.75 ft

c_H horizontal-tail chord, 4.15 ft

D propeller diameter, 4.77 ft

HM flap hinge moment, ft-lb

J propeller advance ratio, $\frac{V}{nD}$

M pitching moment about 0.35 c, ft-lb

n propeller angular velocity, rps

N number of propellers

P	power, ft-lb/sec
q	free-stream dynamic pressure, psf
r	propeller blade station, ft
R	propeller blade radius, ft, and resultant force, lb
RCF	rotating cylinder flap
S	wing area, 128 sq ft
S_f	flap area, 60.5 sq ft
T	thrust, lb
T_c'	thrust coefficient, $\frac{T}{qS}$
U	cylinder peripheral velocity, fps
V	free-stream velocity, fps
V_s	descent velocity, fpm
Y	side force, lb
α	fuselage angle of attack, deg
α_δ	lift effectiveness parameter, $\frac{C_{L_\delta}}{C_{L_\alpha}}$ (ref. 1)
β	propeller blade angle at 0.75R, deg
γ	flight-path angle, deg
δ_A	aft flap deflection, deg
δ_f	flap deflection, deg
δ_T	thrust tilt, deg
δ_W	wing tilt, deg
ϵ	downwash angle, deg
Θ	slipstream turning angle, deg
ρ	mass density of air, slugs/cu ft

LARGE-SCALE WIND-TUNNEL TESTS OF AN AIRPLANE MODEL WITH FOUR PROPELLERS AND ROTATING CYLINDER FLAPS

By James A. Weiberg and Stanley O. Dickinson

Ames Research Center

SUMMARY

Wind-tunnel tests were made of a model equipped with rotating cylinder flaps and four propellers. Comparison with the results obtained with the same flap on a model with two propellers of larger diameter but with approximately the same slipstream coverage on the wing showed that large gains were obtained in the lift due to thrust and slipstream turning as a result of the increased flap chord relative to propeller diameter. The slipstream turning angles for the four-propeller model were approximately equal to the flap deflection.

INTRODUCTION

The small-scale and two-dimensional tests of reference 2 indicated that a rotating cylinder built into the leading edge of a flap could provide large gains in flap lift with low rotating cylinder power, low longitudinal trim requirements, and low flap hinge moments. Based on these data, tests were made of a large-scale, three-dimensional, two-propellered model with a rotating cylinder flap (RCF). The results are presented in reference 3. Additional tests were made of the rotating cylinder flap on a model having four propellers of smaller diameter but providing approximately the same slipstream coverage on the wing.[1] For this model with reduced propeller diameter the ratio of flap chord to propeller diameter was greater than for the model of reference 3 and hence would provide greater slipstream turning as indicated in reference 4. The tests were made in the Ames 40- by 80-Foot Wind Tunnel. The investigation included an examination of the effects of cylinder speed, propeller thrust, nacelle spacing, wing leading-edge slats, wing and nacelle tilt, fuselage strakes, and horizontal-tail location on flap effectiveness, stall characteristics, longitudinal stability, slipstream turning, and descent characteristics.

MODEL

The model for these tests shown in figure 1 incorporated the rotating cylinder flap described in reference 3. The geometry and dimensions of the model are given in figure 2. As shown in this figure, two nacelle locations

---

[1]Professor A. Alvarez-Calderon was a consultant for the design of the rotating cylinder flap used on both the two and the four-propellered models.

were tested on the model. The wing could be tilted 20° leading edge up and the nacelles could be tilted 15° nose down. The pivot axes are shown in figure 2.

Details of the flap are shown in figures 1(c) and 2(b). A 10.9-inch-diameter machined aluminum cylinder (0.25-inch wall) was built into the leading edge of the flap. The cylinder was in four segments, each 65.1 inches long and driven by an electric motor. Each segment had 18.2-inch-diameter disks on the ends at the wing tips and fuselage. The cylinder segments were separated 0.25 inch and fitted with 13.4-inch-diameter disks at mid-semispan. The flap included a slotted aft portion with a chord that was 28 percent of the wing chord.

The horizontal tail could be located in two positions representing a low and a tee tail. These positions are shown in figure 2(a).

Details of the wing leading-edge slat, end plates, nacelle fairings, and fuselage strakes are shown in figure 2.

The model had 4 three-bladed propellers of 4.77-foot diameter driven by electric motors. The geometry of the propeller blades is shown in figure 3(a). The blade angle at 0.75 blade radius was 21.5°.

TESTS AND CORRECTIONS

Tests were made at free-stream dynamic pressures from 0 to 2.6 psf (Reynolds number = 1.5 million). The data from these tests include the direct propeller forces as well as the aerodynamic forces. The propeller characteristics are given in figures 3(b) and 3(c). Forces and moments are presented about the wind axes for a moment center located as shown in figure 2(b).

Tunnel-wall corrections were not applied to the data because the relative size of the model and the wind tunnel was within the boundaries indicated in reference 5 for best correlation between wind-tunnel and flight-test results. The conventional tunnel-wall corrections are:

$$\alpha = \alpha_u + 0.3\ C_L$$

$$C_D = C_{D_u} + 0.0052\ C_L^2$$

where the subscript u stands for uncorrected data.

No corrections were made for effects of the model supports as these effects were estimated to be small ($C_{D_{tare}} = 0.027$).

Cylinder rotational power input was determined from measurements of electrical power input to the drive motors and corrected for motor efficiency obtained from a dynamometer calibration of the motors.

Flap hinge moments were obtained from measurements with strain gages on the flap actuator arms.

RESULTS AND DISCUSSION

The data are presented in figures 4 to 27 as listed in table 1.

Flap Effectiveness

The effect of cylinder rotation on lift is shown in figure 4. Cylinder speed is expressed as a ratio of cylinder surface speed to free-stream velocity U/V. At low values of U/V, lift increases rapidly with increasing U/V until the flow on the flap is attached, corresponding to the knees of the curves in figure 4. The ratio U/V for attached flow for a given flap deflection was the same as for the two-propellered model of reference 3. The ratio U/V for attached flow was dependent only on flap deflection and was independent of angle of attack, propeller slipstream effects, wing tilt, nacelle tilt, and nacelle spacing.

For the remainder of the figures wherein U/V is constant, the value of U/V given on the figures and in table 1 is at or above the value for attached flow. The power required to rotate the cylinder is shown in figure 5(a) and is the same as for the two-propeller model of reference 3. Figures 5(b) and 5(c) show the relationship between cylinder speed, airspeed, and U/V.

Lift and drag due to flap deflection and thrust are shown in figure 6. The data in this figure are for a value of U/V at or above that required for attached flow on the flap. At zero thrust, the lift due to flap deflection shows reasonable agreement with the flap theory of reference 1 for flap deflections up to 70°. The apparent deterioration of flap effectiveness above 70° may be due to wing-fuselage juncture effects since tufts showed attached flow on the flap except near the fuselage, and the presence of large external vortices on the fuselage and nacelles.

The lift due to thrust for 60° flap deflection is compared in figure 7 with the two-propeller data from reference 3. The lift due to thrust was greater for the model with the four propellers because of the greater turning of the slipstream for the larger ratio of flap chord to propeller diameter. Included in figure 7 are estimated values from reference 4 and comparisons with a blowing BLC flap from reference 6. For the same flap chord to propeller diameter ratio, the lift due to thrust is the same for the RCF and the blowing BLC flap and is estimated reasonably well by the theory of reference 4.

The ability of the aft flap to provide lift control is shown in figure 8 for a 60° main flap deflection. An aft flap deflection of 20° provides a capability of about 0.13 g normal acceleration. Above 20° deflection, the effectiveness decreased. At high thrust coefficients, the aft flap is more effective for drag control than lift control.

Stall Characteristics

Observations of the flow about the wing, flaps, and fuselage with tufts and streamers indicated that maximum lift appeared to be limited by fuselage flow deterioration rather than flap or wing stall. Various attempts were made to contain or delay this flow interference to higher angles of attack by the use of slats, reduced nacelle spacing, wing tilt, and fuselage strakes.

To increase the propeller slipstream coverage near the fuselage, the nacelles were moved inboard (nacelle spacing B, fig. 2(a)). The effect of the reduced nacelle spacing with 70° flap deflection is shown in figure 9. The comparison shown in this figure also includes the effect of propeller rotation; however, figure 13(a) shows that, at least for 80° flap deflection, this effect would be small. Figure 9 thus indicated that, at a thrust coefficient of 4, the closer nacelle spacing improved the flow over the wing and flap near the fuselage and increased maximum lift.

The effect of full-span, wing leading-edge slats is shown in figure 10. With 60° flap deflection, the slats increased maximum lift at thrust coefficients of 2 or less. With a higher thrust coefficient or higher flap deflection the full-span slat was detrimental. It is not known if the slat would be more effective if tailored to the higher thrust coefficients. Also, tested were partial span slats between the inboard nacelles and the fuselage on the model with the reduced nacelle spacing (nacelle spacing B, fig. 2(a)) and flaps 70°. This slat configuration did not improve lift or stall characteristics (fig. 10(c)).

The effect of wing tilt is shown in figure 11. The data in this figure show that the wing attitude relative to the fuselage did not appear to affect the wing maximum lift capability with flaps deflected.

An attempt was made to improve the flow around the large angular fuselage by large strakes on the forward lower part of the fuselage (fig. 2(a)). These strakes improved the fuselage flow and increased maximum lift as shown in figure 12.

The effect of direction of propeller rotation on stall characteristics was also investigated. Two modes of rotation were tested: all like rotation, and with all inboard blades down going. The results are shown in figure 13. The counterrotating arrangement with down-going blades next to the fuselage reduced flow separation in that region but did not affect the longitudinal force characteristics. The counterrotating propeller arrangement, however, greatly reduced the side-force variation with angle of attack (fig. 13(b)) similar to the results shown in reference 7.

Longitudinal Stability and Control

The effect of horizontal-tail location on stability is shown in figure 14 for a flap deflection of 80°. Large variations in the tail-on stability $\partial C_m/\partial C_L$ are caused by changes in the downwash parameter $\partial\varepsilon/\partial\alpha$ with T_c' (similar to the results shown in ref. 6).

The model with the low tail shows larger variations of $\partial C_m/\partial C_L$ with T_c' and becomes unstable at high T_c' (moment center at 0.35 c). The magnitude of the tail pitching-moment contribution was approximately the same for both tail positions. For flap deflections of 60° or less at low angles of attack (figs. 17 and 18), the model with the low tail was unstable, even with power off ($T_c' = 0$). The results of reference 8 indicate that this may be the result of the wing-fuselage wake impinging on the tail. The tee tail provided a positive contribution to stability (fig. 14(b)).

Zero Airspeed Characteristics

A measure of the effectiveness of a flap is its ability to convert thrust into lift by deflection of the slipstream. The slipstream turning effectiveness at zero forward speed is shown in figure 15. Included in this figure are estimated values from reference 4, comparisons with the two-propeller RCF data of reference 3, and data for a four-propeller blowing BLC flap from reference 6. The RCF on the four-propeller model with a larger flap chord relative to the propeller diameter provided greater slipstream turning for a given flap deflection than either the RCF on the two-propeller model or the blowing BLC flap. The data in figure 15 are plotted with flap deflection referenced to thrust axis and show that slipstream turning at zero airspeed is a function of the flap deflection relative to the thrust axis. On the four-propeller RCF model, 74° slipstream turning at 87-percent thrust recovery was obtained with 70° flap deflection (aft flap deflected 20°).

The rotating cylinder flap model provided a given slipstream turning with less pitching moments than the blowing BLC flap. With the four-propeller RCF model, these moments were zero for a moment center located at 0.35 c.

The data in figure 15 indicate that the model with 80° flap deflection can hover with approximately 20° angle of attack or wing tilt. At forward flight for the model with the wing tilted, minimum drag occurs at a large negative fuselage angle of attack (fig. 23(b)). Less negative fuselage angle of attack is required with negative flap deflection.

Descent Characteristics

The effects of flaps, slats, and wing and thrust tilt on the descent characteristics are shown in figure 16. In this figure, the descent angle and descent velocity V_s at $C_{L_{max}}$ are shown as functions of flap deflection for an assumed wing loading W/S of 40 psf. Figure 16 shows that the descent angle at $C_{L_{max}}$ increased with both main flap and aft flap deflection.

Additional gains in descent capability can be obtained if the inboard and outboard propellers are operated at different thrust settings to vary the spanwise distribution of lift and drag as shown in reference 8. The spanwise distribution of thrust was varied by operating the propellers at different rotational speeds with the blade angle held constant. The effect of differential

propeller thrust on the descent angles and descent velocity at $C_{L_{max}}$ is shown in figure 16(c). The differential propeller thrust, for approximately the same average total thrust, resulted in a loss in lift (fig. 27). Drag at maximum lift, however, was increased giving an increase in descent angle of about 4° (fig. 16(c)). Descent angles of over 20° were obtained at maximum lift.

CONCLUDING REMARKS

The results have shown that the rotating cylinder flap can provide the large values of slipstream turning and lift due to thrust indicated by the large flap chord relative to propeller diameter. Hover could be achieved with moderate amounts of angle of attack or wing incidence. At forward velocities, the drag due to wing incidence could be reduced by small amounts of negative flap deflection. Fuselage flow deterioration appeared to limit maximum lift and could reduce the effectiveness of the horizontal tail for some vertical locations. The effects of this flow deterioration could be reduced by fuselage strakes and by the spacing between the propellers and fuselage.

Ames Research Center
National Aeronautics and Space Administration
Moffett Field, Calif. 94035, Dec. 10, 1969

REFERENCES

1. DeYoung, John: Theoretical Symmetric Span Loading Due to Flap Deflection for Wings of Arbitrary Plan Form at Subsonic Speeds. NACA Rep. 1071, 1952. (Supersedes NACA TN 2278.)

2. Alvarez-Calderon, Alberto; and Arnold, Frank R.: A Study of the Aerodynamic Characteristics of a High-Lift Device Based on a Rotating Cylinder and Flap. Stanford University Tech. Rep. RCF-1, 1961.

3. Weiberg, James A.; and Gamse, Berl: Large-Scale Wind-Tunnel Tests of an Airplane Model With Two Propellers and Rotating Cylinder Flaps. NASA TN D-4489, 1968.

4. Kuhn, Richard E.: Semiempirical Procedure for Estimating Lift and Drag Characteristics of Propeller-Wing-Flap Configurations for Vertical- and Short- Take-Off-and-Landing Airplanes. NASA MEMO 1-16-59L, 1959.

5. Cook, Woodrow L.; and Hickey, David H.: Comparison of Wind-Tunnel and Flight-Test Aerodynamic Data in the Transition-Flight Speed Range for Five V/STOL Aircraft. Paper 26, NASA SP-116, 1966.

6. Weiberg, James A.; and Page, V. Robert: Large-Scale Wind-Tunnel Tests of an Airplane Model With an Unswept, Aspect-Ratio-10 Wing, Four Propellers, and Blowing Flaps. NASA TN D-25, 1959.

7. Weiberg, James A.; and Giulianetti, Demo J.: Large-Scale Wind-Tunnel Tests of an Airplane Model With an Unswept Tilt Wing of Aspect Ratio 5.5, and With Various Stall Control Devices. NASA TN D-2133, 1964.

8. Deckert, Wallace H.; Page, V. Robert; and Dickinson, Stanley O.: Large-Scale Wind-Tunnel Tests of Descent Performance of an Airplane Model With a Tilt Wing and Differential Propeller Thrust. NASA TN D-1857, 1964.

TABLE 1.- FIGURE INDEX

Figure	Data	δ_f	δ_A	$\left(\frac{U}{V}\right)_{nom}$	Tail	Slats	T_c'	δ_w	δ_T	Propeller rotation
4	C_L vs. U/V									
5	Power required									
6	ΔC_L vs. δ_f									
7	ΔC_L vs. T_c'									
8	ΔC_L vs. δ_A									
	Effect of:									
9	Nacelle spacing									
10	Slats									
11	Wing tilt									
12	Strakes									
13	Propeller rotation									
14	Horizontal tail									
15	Slipstream turning									
16	Descent characteristics									
	Configuration A									
17(a)	C_D, α, C_m vs. C_L	40	0	5	low, off	off	0-4	0	0	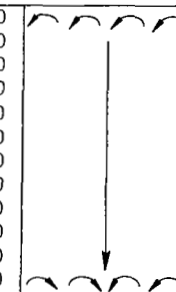
17(b)		40	10	6.6	off	off	0-4	0	0	
17(c)		40	10	6.6	off	on	0-4	0	0	
18(a)		60	0	6.6	off	off	0-6	0	0	
18(b)		60	0	6.6	off	on	0-4	0	0	
18(c)		60	0	6.6	low	off	0-4	0	0	
18(d)		60	0	6.6	low	on	0-4	0	0	
18(e)		60	20	6.6	off	off	0-6	0	0	
18(f)		60	30	6.6	off	on, off	0-4	0	0	
18(g)		60	30	6.6	low	off	0-4	0	0	
19(a)		70	0	6.6	off	off	0-6	0	0	
19(b)		70	0	6.6	tee	off	0-4	0	0	
19(c)		70	20	6.6	off	off	0-6	0	0	
19(d)		70	20	6.6	off	on	0-6	0	0	
19(e)		70	20	6.6	tee	off	0-4	0	0	
20(a)		80	0	0	low	off	0-8	0	0	
20(b)		80	0	6.6	off	off	0-6	0	0	
20(c)		80	0	6.6	off	on	0-4	0	0	
20(d)		80	0	6.6	tee	off	0-4	0	0	
20(e)		80	0	6.6	tee	off	0-4	0	0	
20(f)		80	0	6.6	low	off	0-4	0	0	
21	C_{h_f} vs. α	40, 70	10, 20	6.6	off	off	0-4	0	0	
	Configuration B									
22(a)	C_D, α, C_m vs. C_L	0	0	0	off	off	0-2	0	0	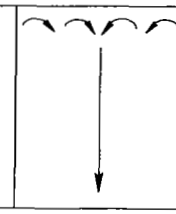
22(b)		0	0	0	off	off	0-2	20	0	
23		-10	-10	0	off	off	0-2	20	0	
24		25	10	4	off	off	0-4	20	-15	
25		55	20	6.6	off	off	0-6	20	-15	
26(a)		70	20	6.6	off	off	0-6	0	0	
26(b)		70	20	6.6	off	off	0-6	20	0	
27		70	20	6.6	off	off	(a)	20	0	

[a]Differential thrust T_c' = 8 inboard, 0 outboard and
T_c' = 4 inboard, 0 outboard

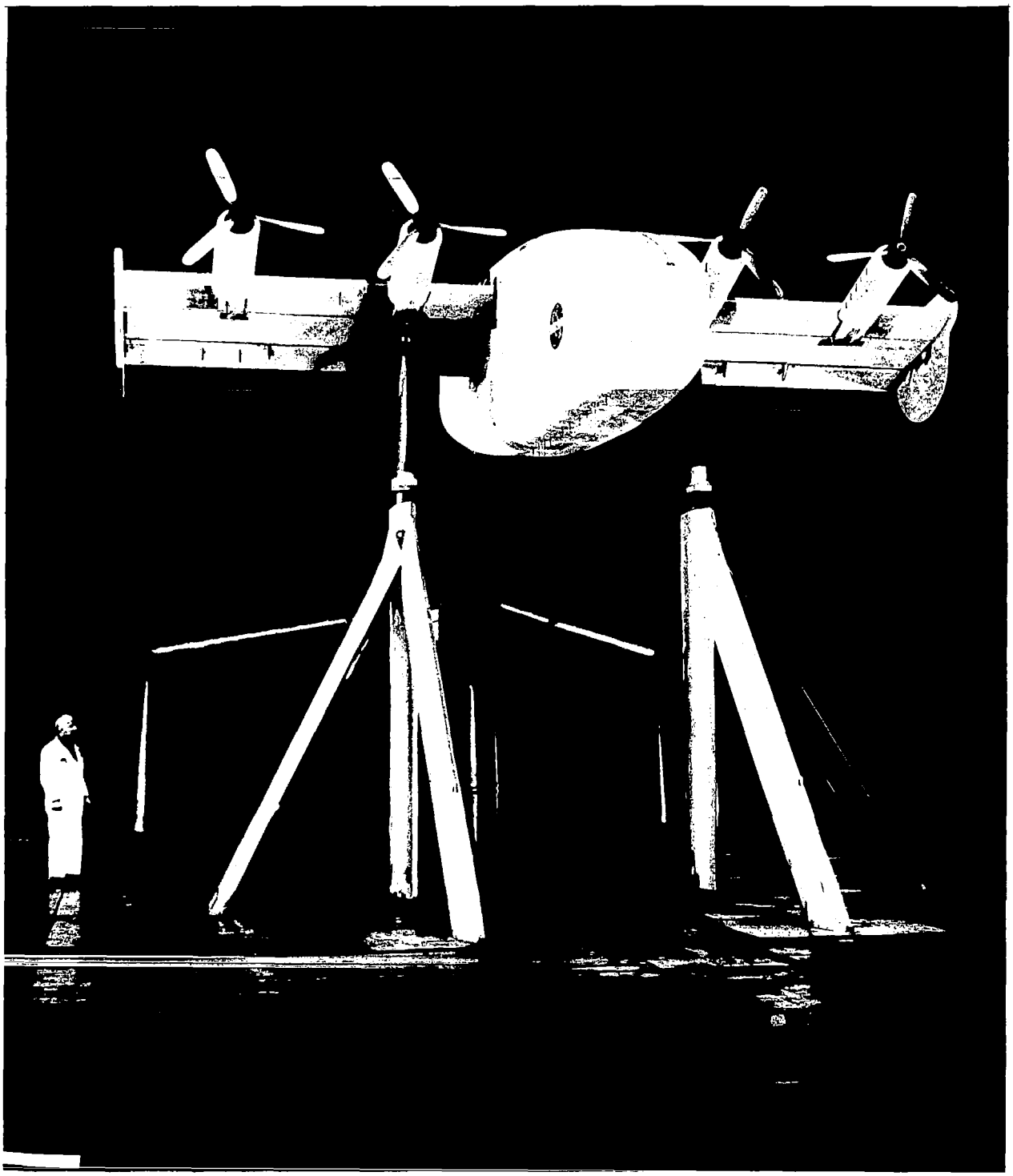

A-40375.1

(a) The model with wing tilted and flaps 0°.

Figure 1.- The model installed in the Ames 40- by 80-Foot Wind Tunnel.

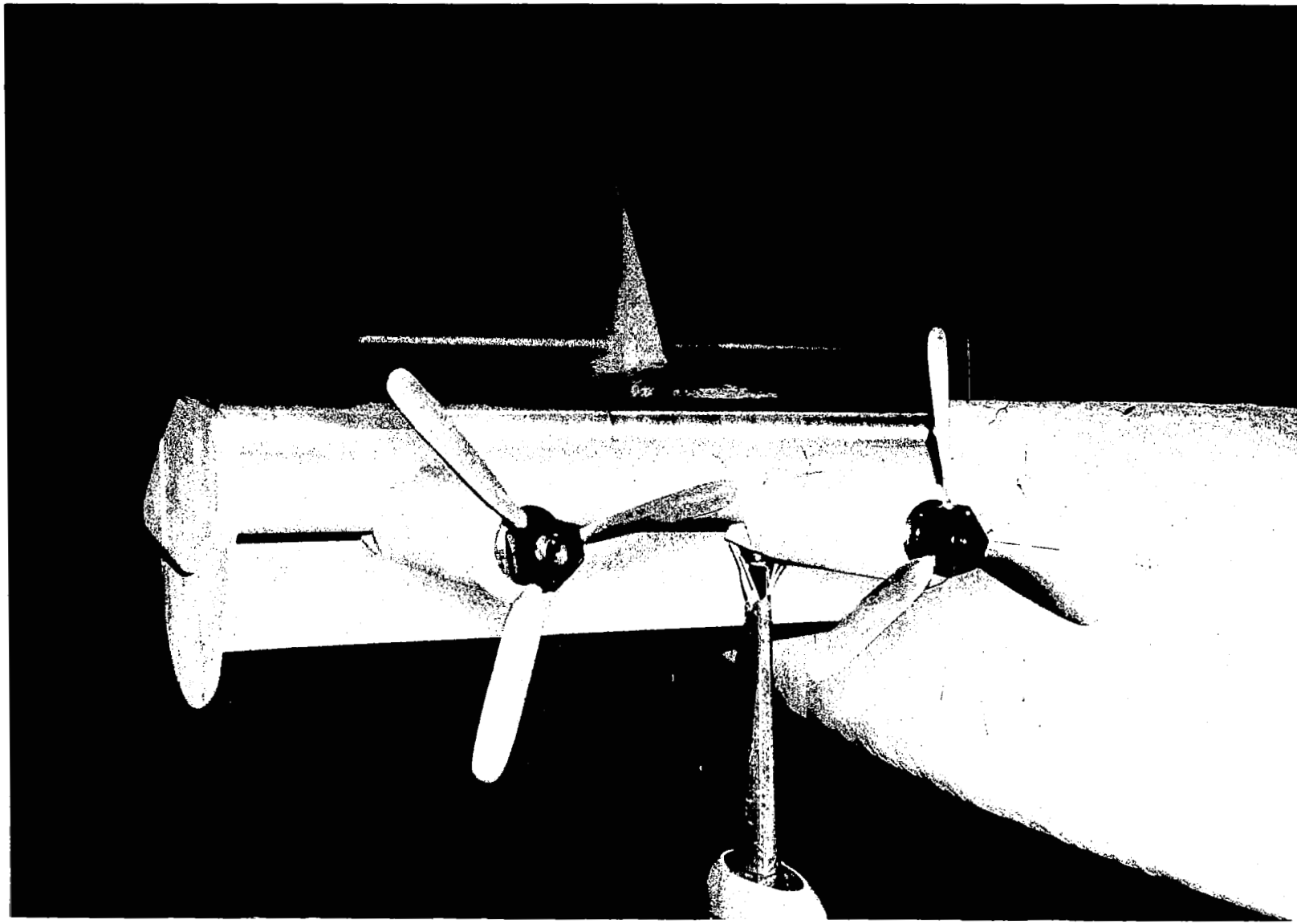

A-39265.1

(b) Front detail of wing and cylinder.

Figure 1.- Continued.

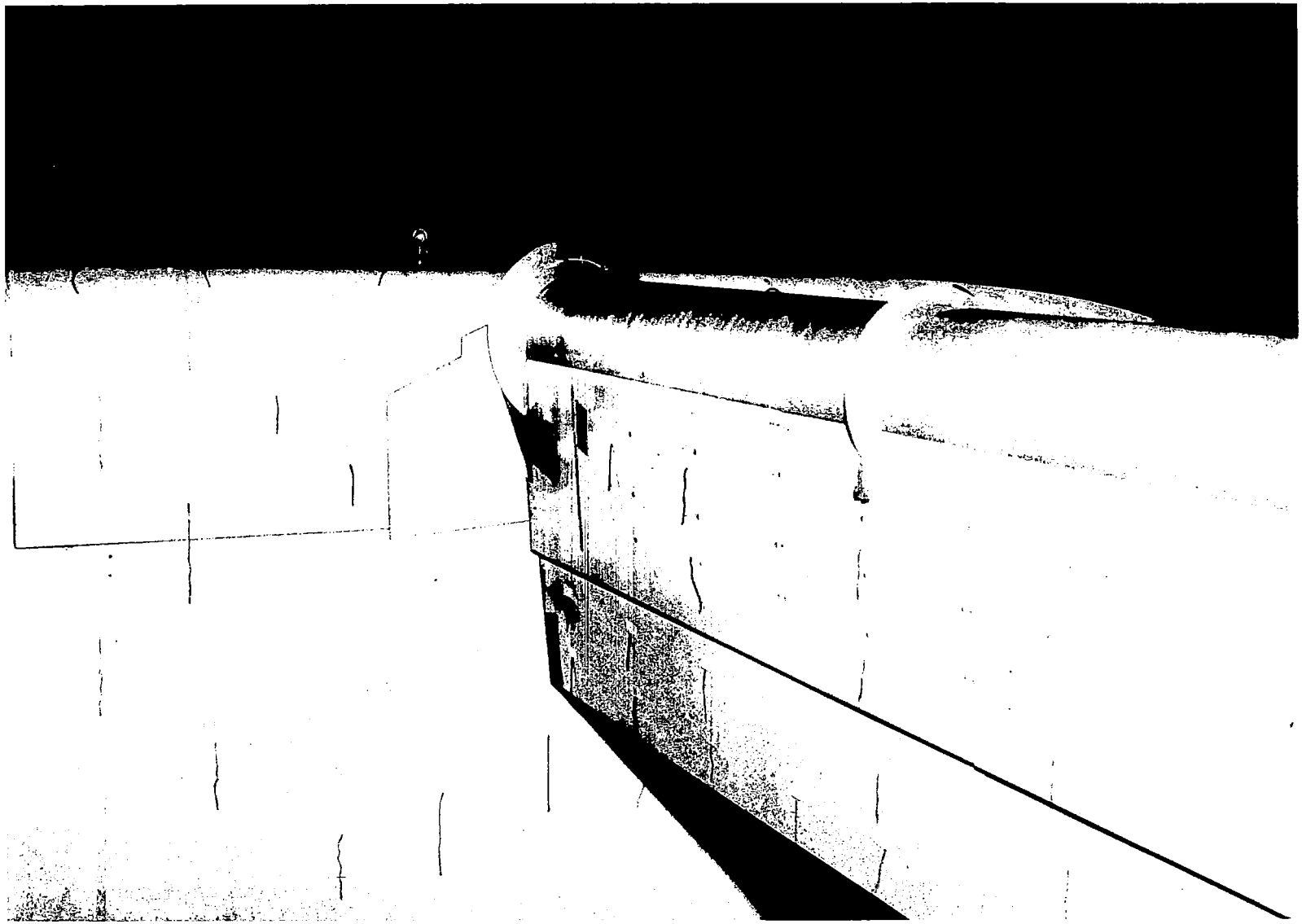

A-39266.1

(c) Rear detail of cylinder and flap.

Figure 1.- Concluded.

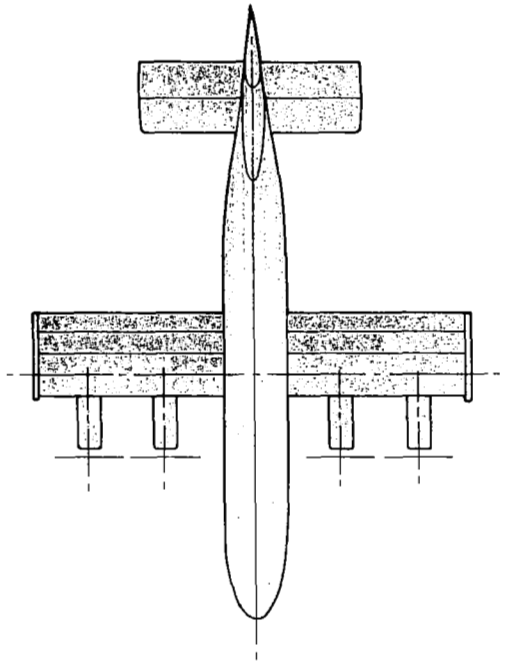

Dimensions in feet

Wing		
Area	128.0	
Span	26.17	
Chord	4.89	
Aspect ratio	5.35	
Section	NACA 5321 (mod.)	
Horizontal tail		
Area	54.0	
Span	13.0	
Chord	4.15	
Aspect ratio	3.26	
Section	NACA 63-216 (inv.)	
Tail length		
Low	15.50	
Tee	18.75	
Location of $c_H/4$	Sta.	WL
Low	30.3	5.5
Tee	33.6	13.5
Nacelle spacing	L_1	L_2
A	10.92	21.40
B	9.25	19.73

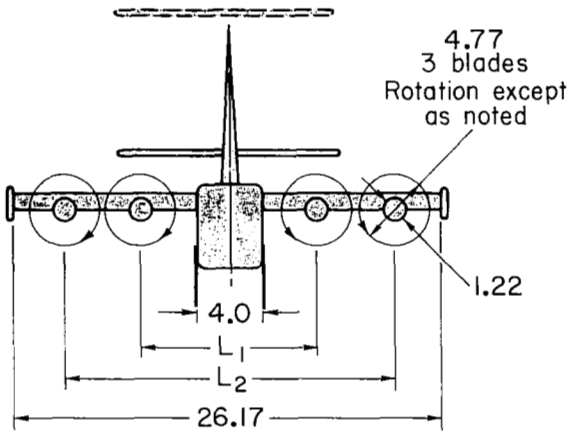

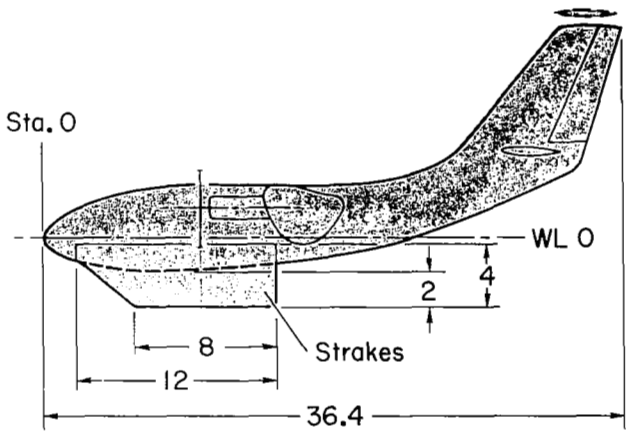

(a) General dimensions.

Figure 2.- Geometry of the model.

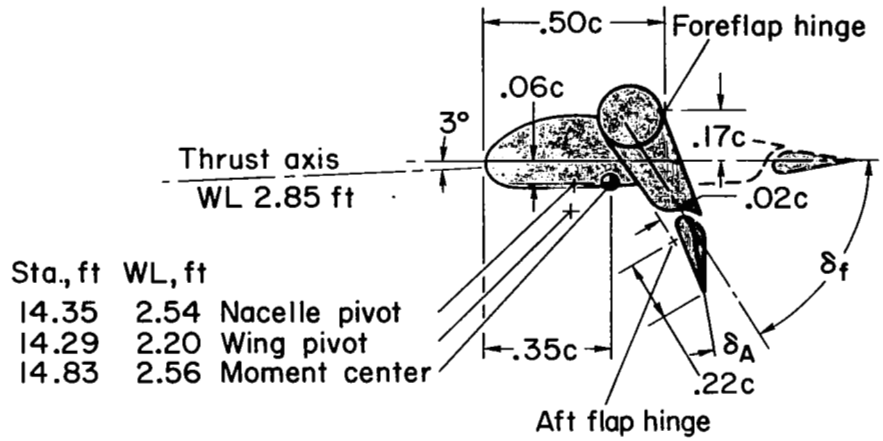

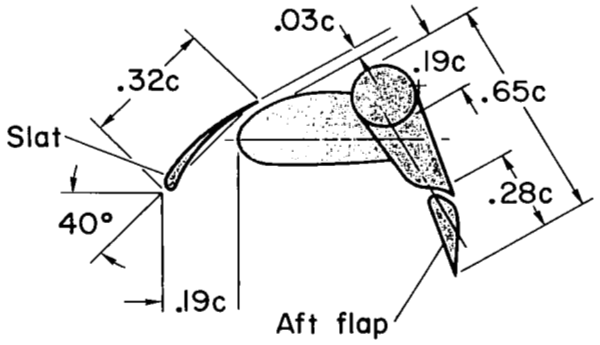

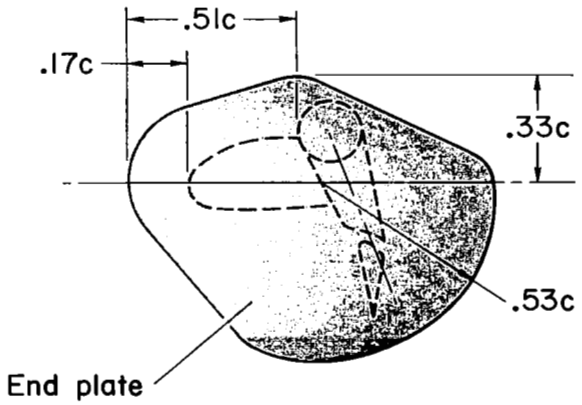

(b) Flap, slat, and end-plate geometry.

Figure 2.- Concluded.

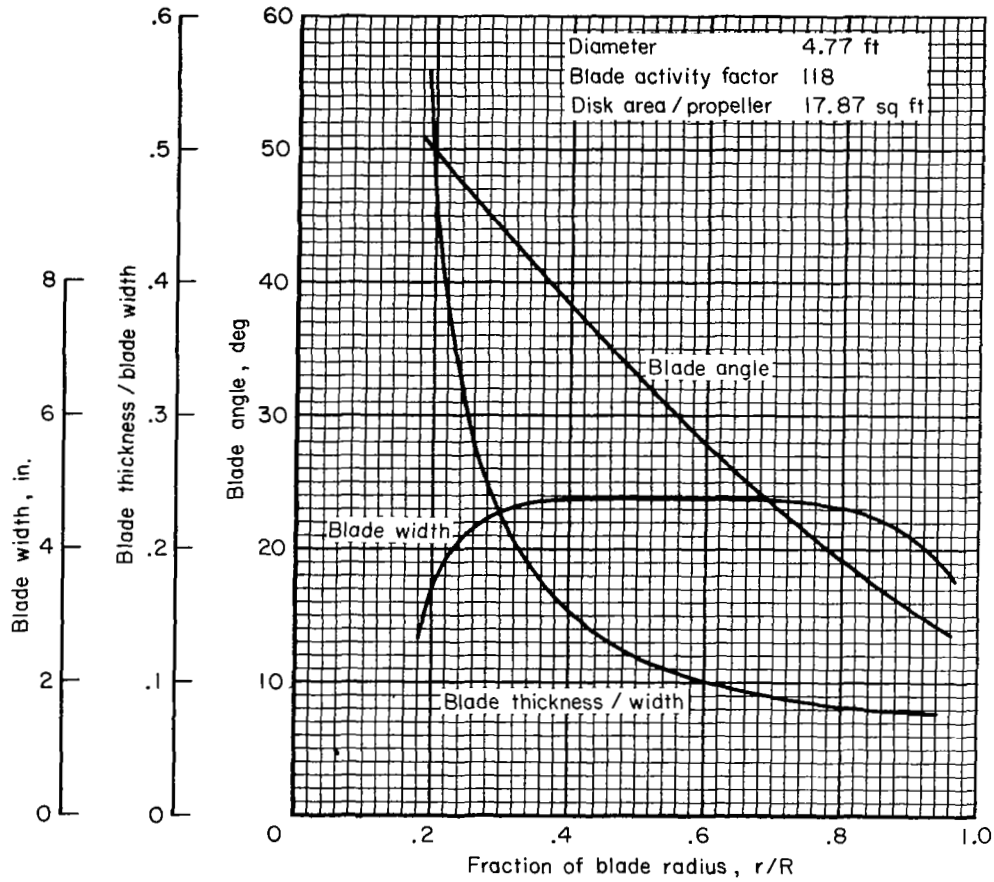

(a) Blade geometry.

Figure 3.- Propeller characteristics.

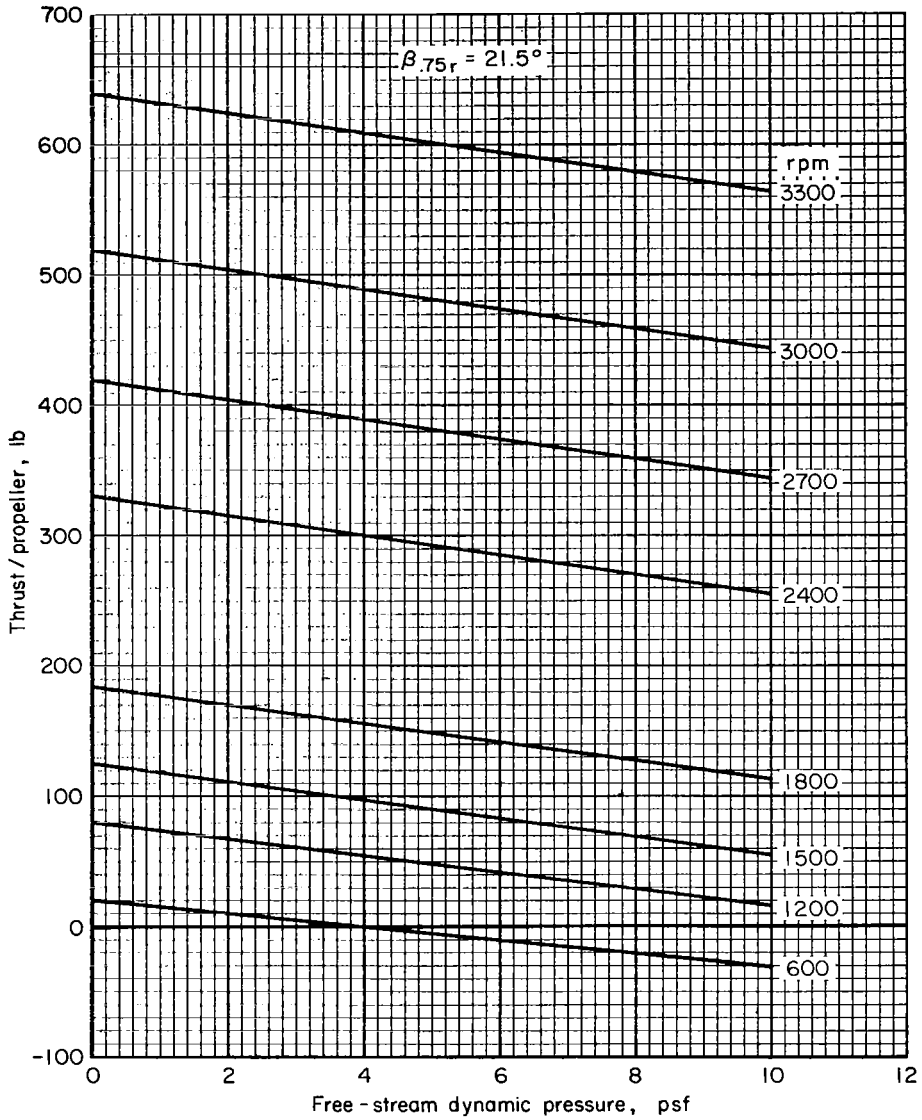

(b) Thrust.

Figure 3.- Continued.

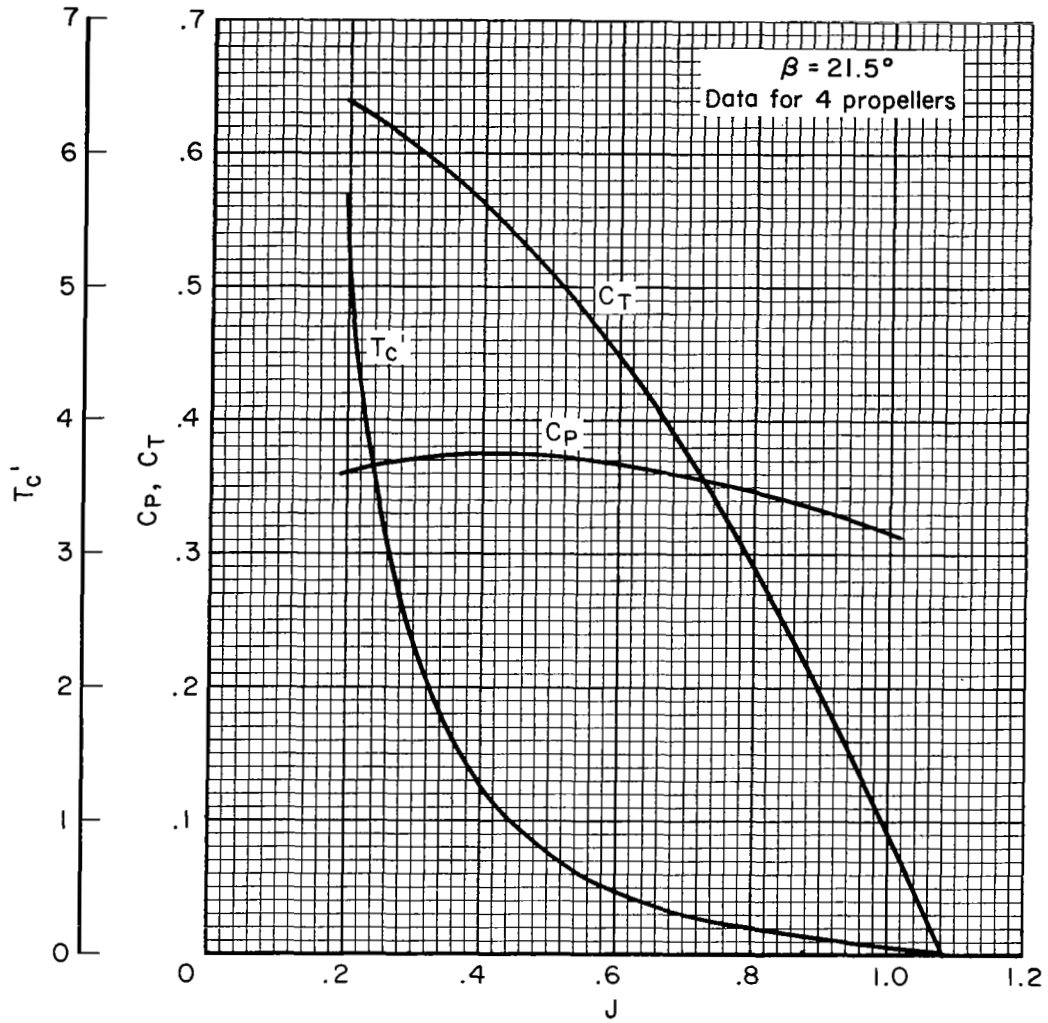

(c) C_T, C_p, T_c'

Figure 3.- Concluded.

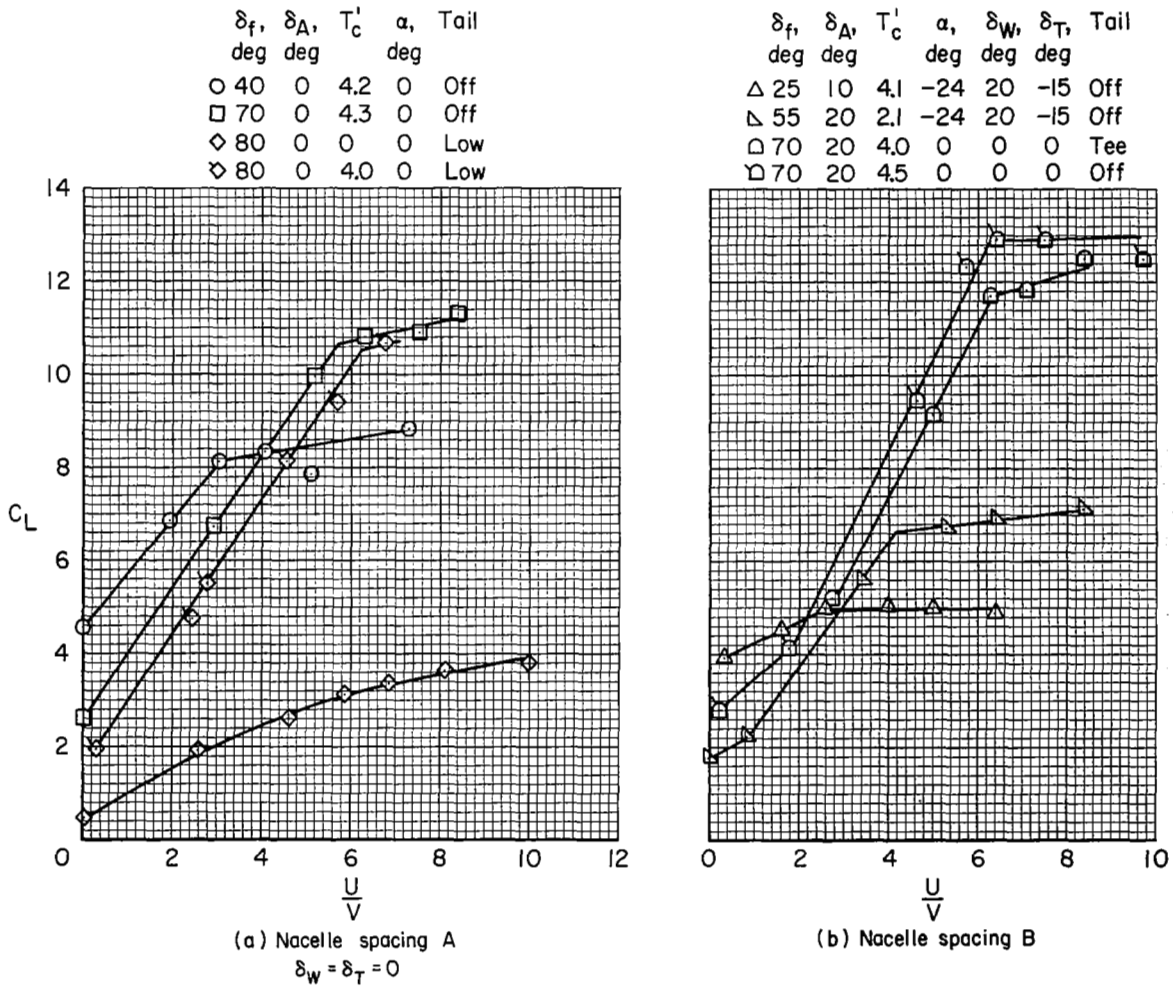

Figure 4.- Effect of cylinder rotation on lift.

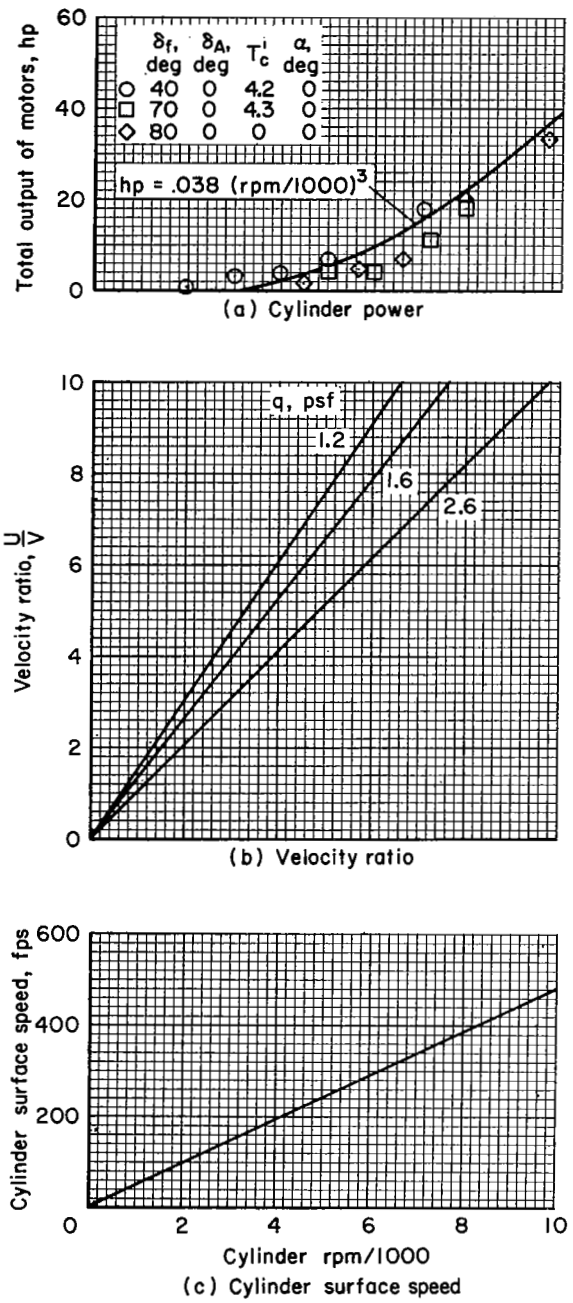

Figure 5.- Cylinder power requirements.

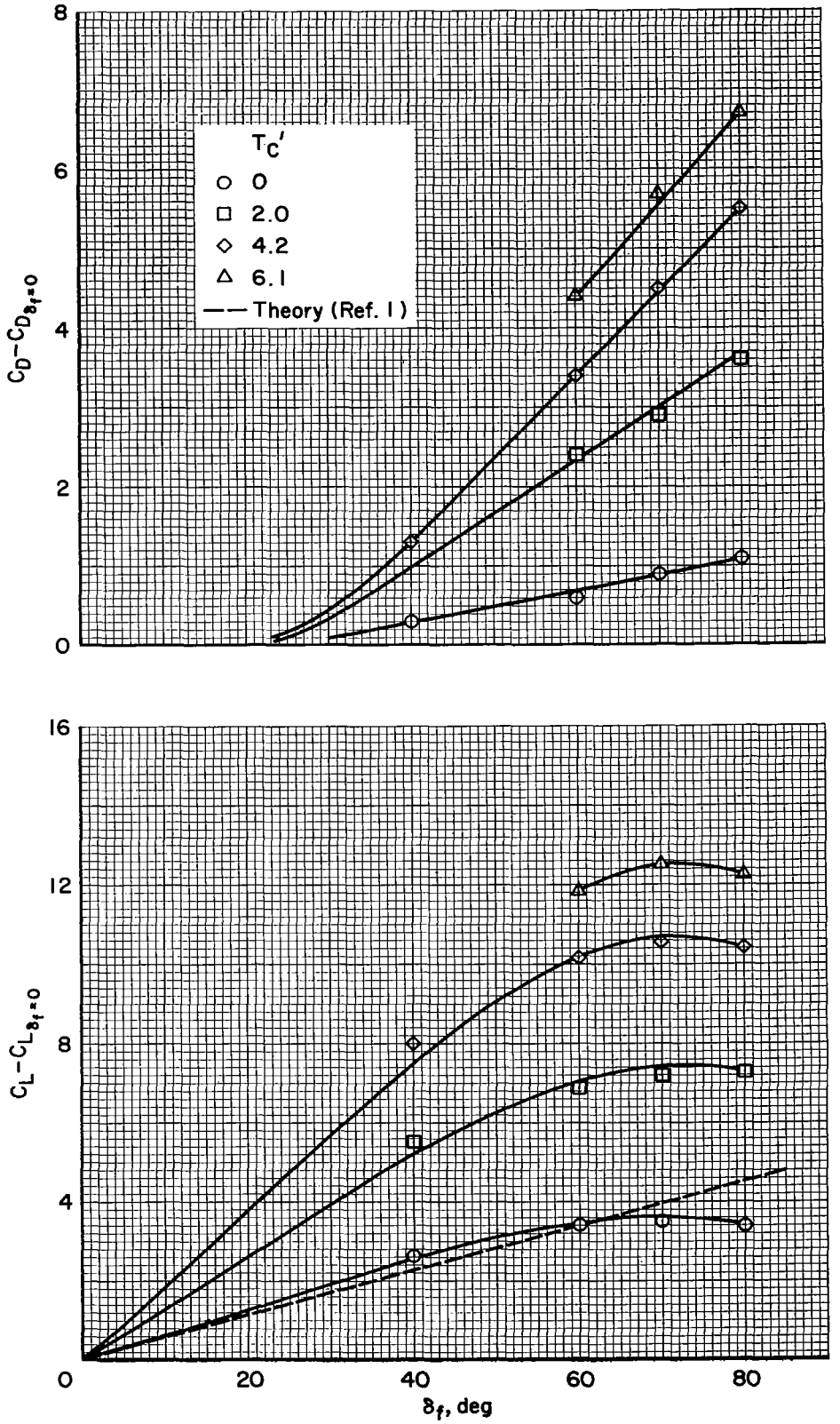

Figure 6.- Flap effectiveness; $\alpha = -5°$.

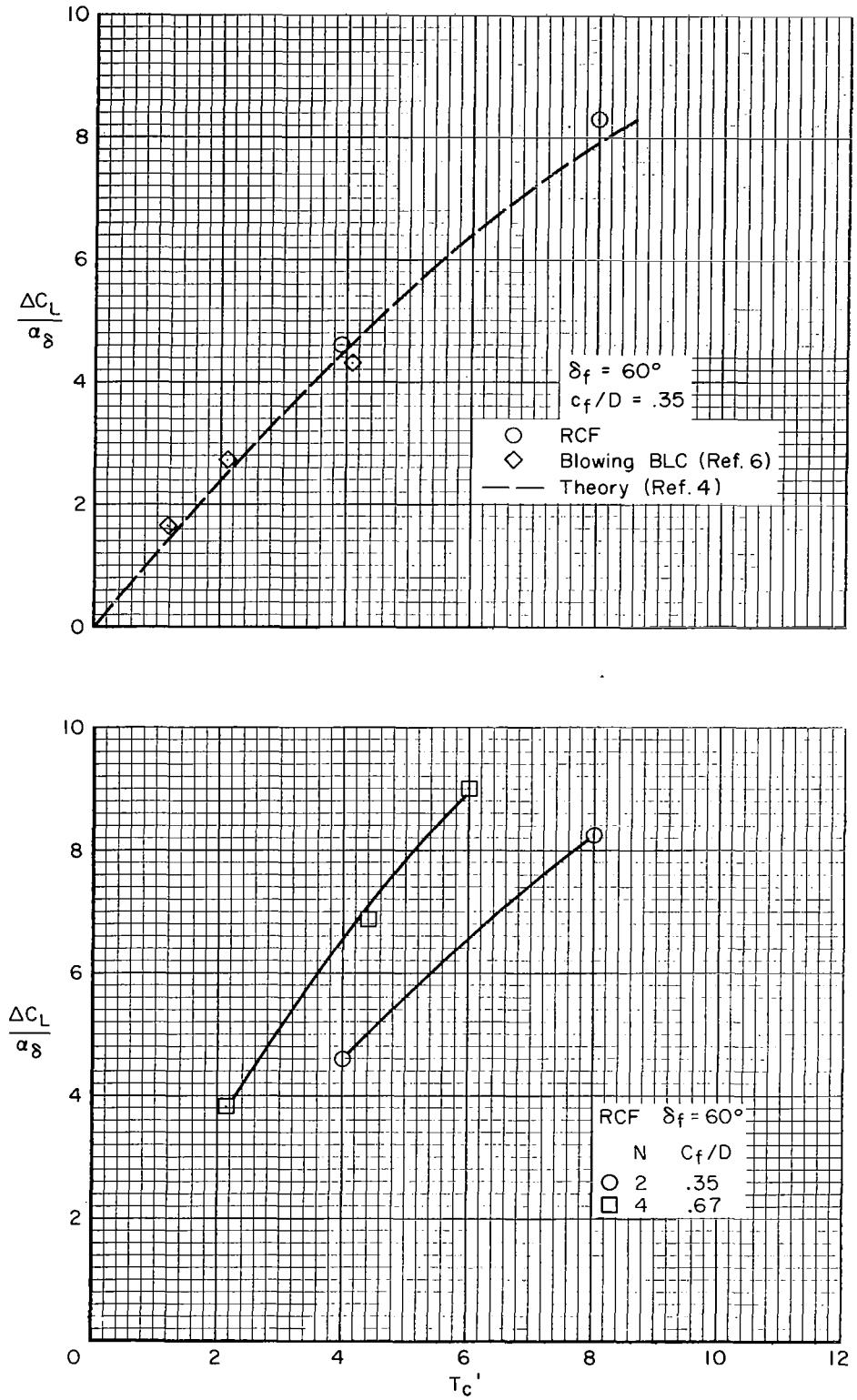

Figure 7.- Lift due to thrust.

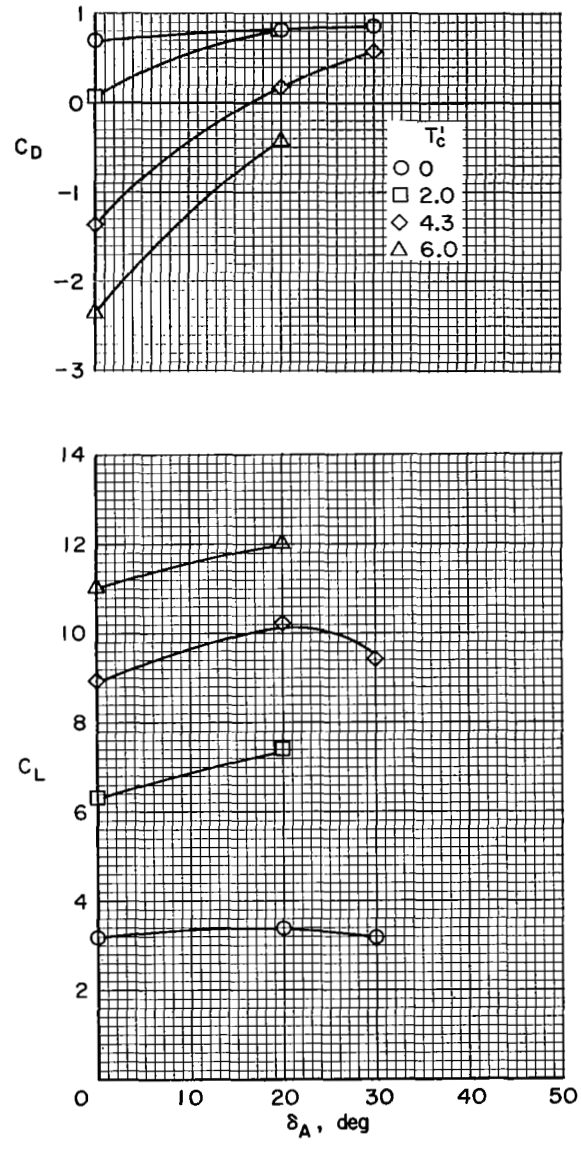

Figure 8.- Effect of aft flap deflection; $\delta_f = 60°$, $\frac{U}{V} = 6.6$, $\alpha = -10°$.

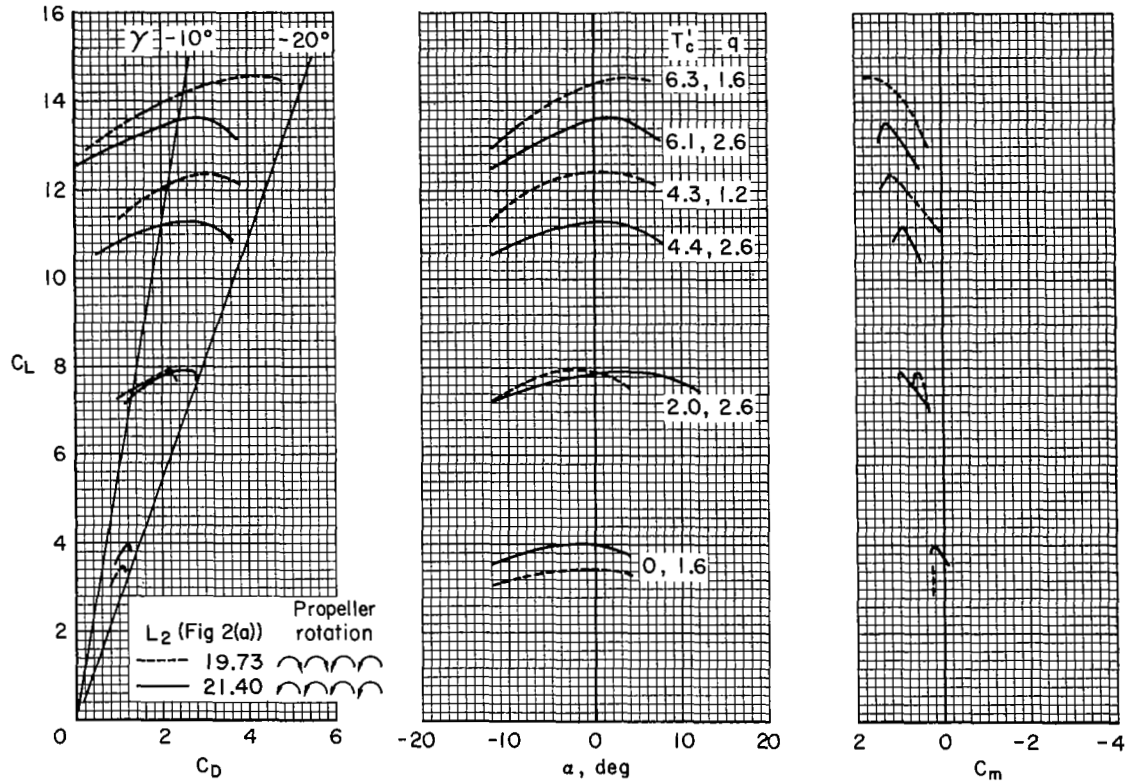

Figure 9.- Effect of nacelle spacing; $\delta_f = 70°$, $\delta_A = 20°$, $\frac{U}{V} = 6.6$, tail off.

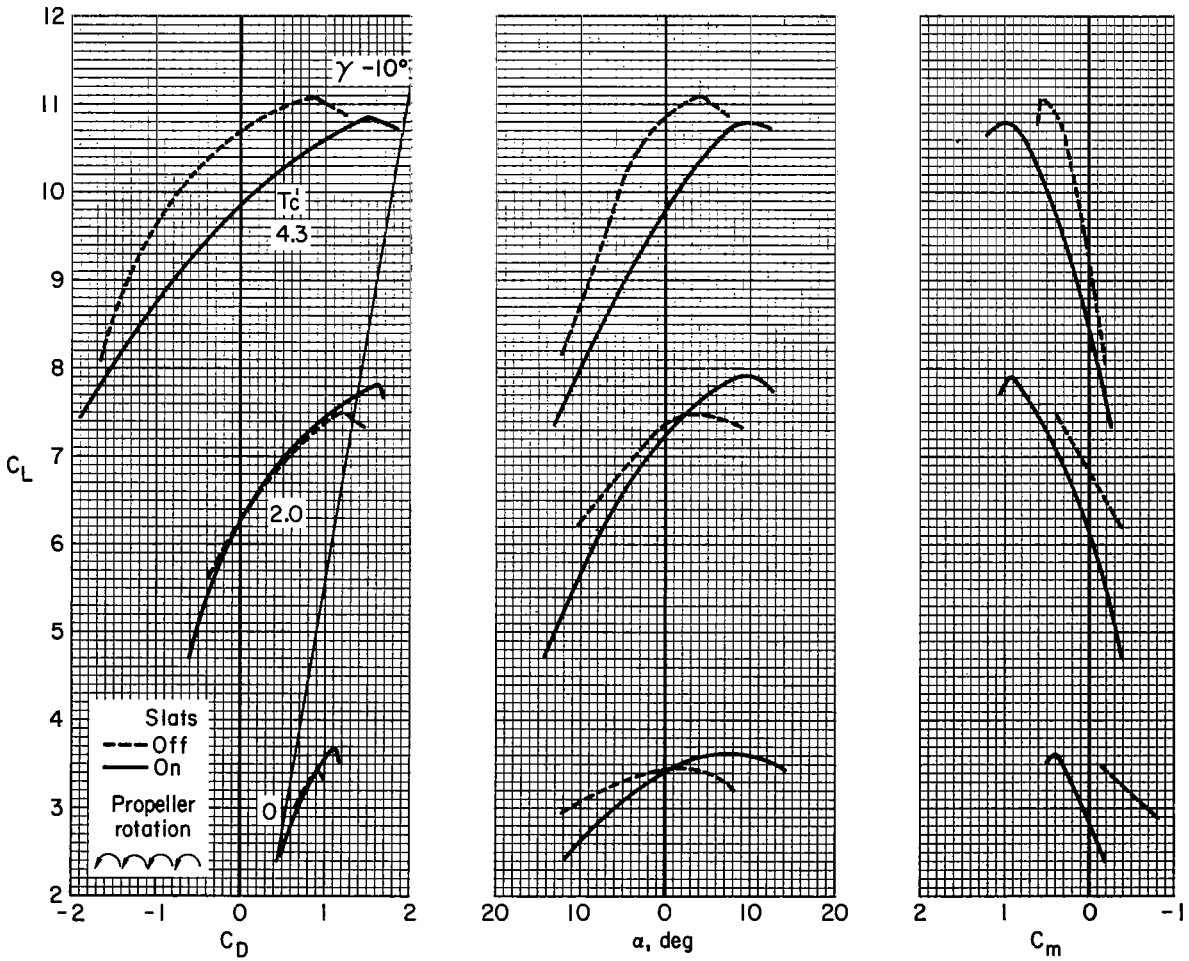

(a) $\delta_f = 60°$; $\delta_A = 0°$, tail off.

Figure 10.- Effect of slats; nacelle spacing A, $\frac{U}{V} = 6.6$.

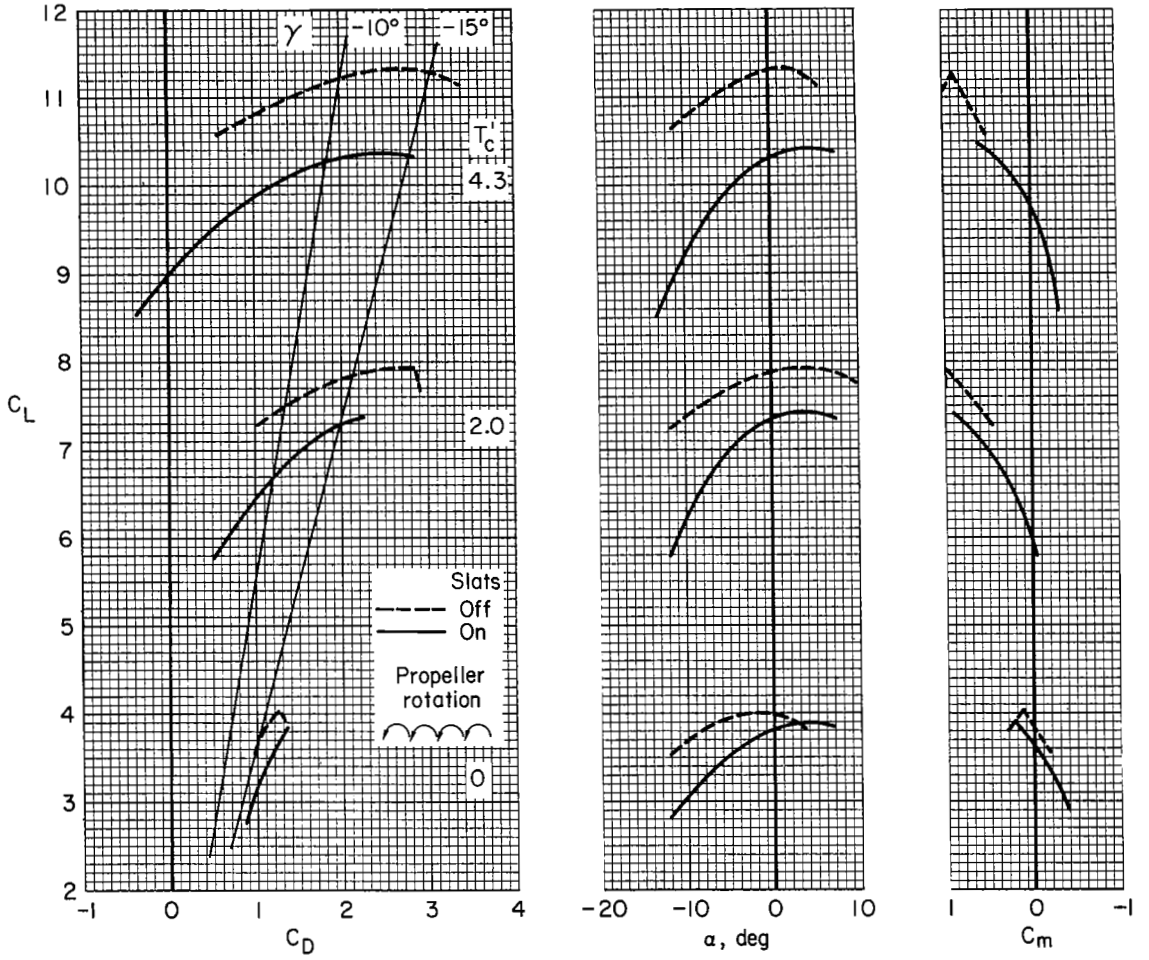

(b) $\delta_f = 70°$; $\delta_A = 20°$, tail off.

Figure 10.- Continued.

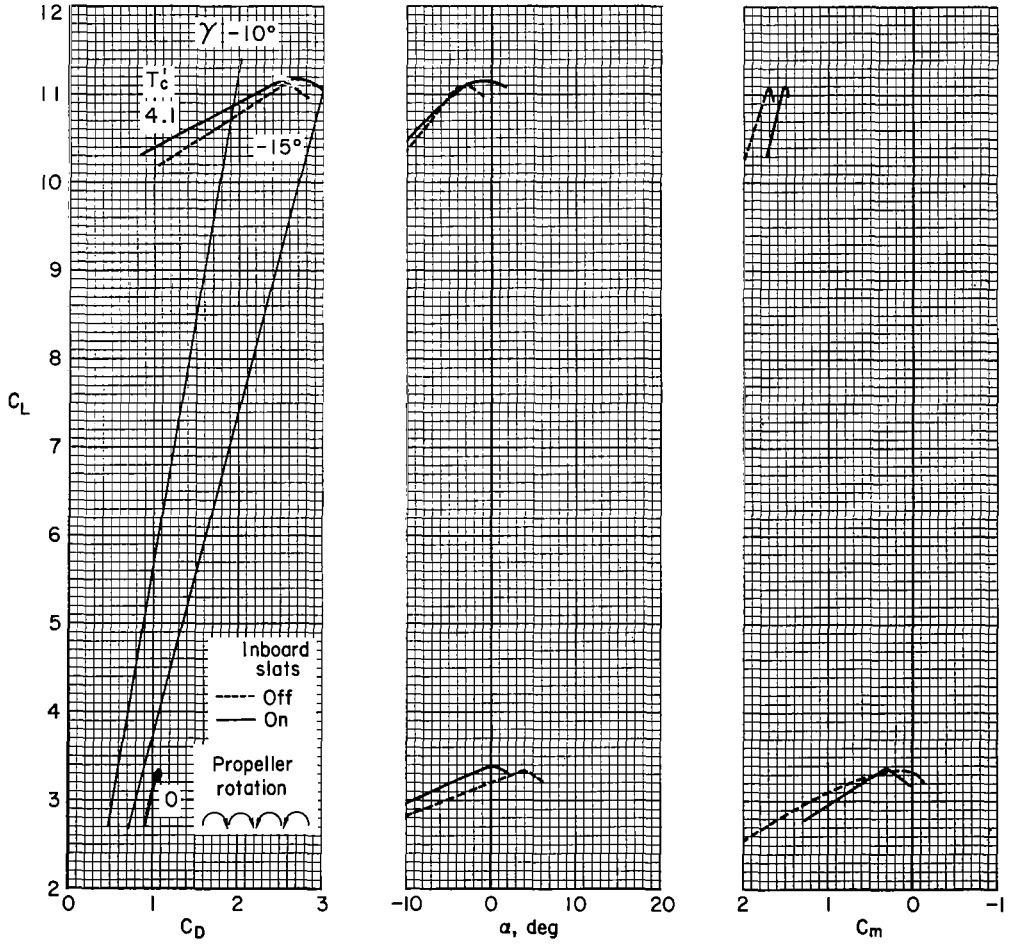

(c) Inboard slats; $\delta_f = 70°$, $\delta_A = 20°$, tee tail.

Figure 10.- Concluded.

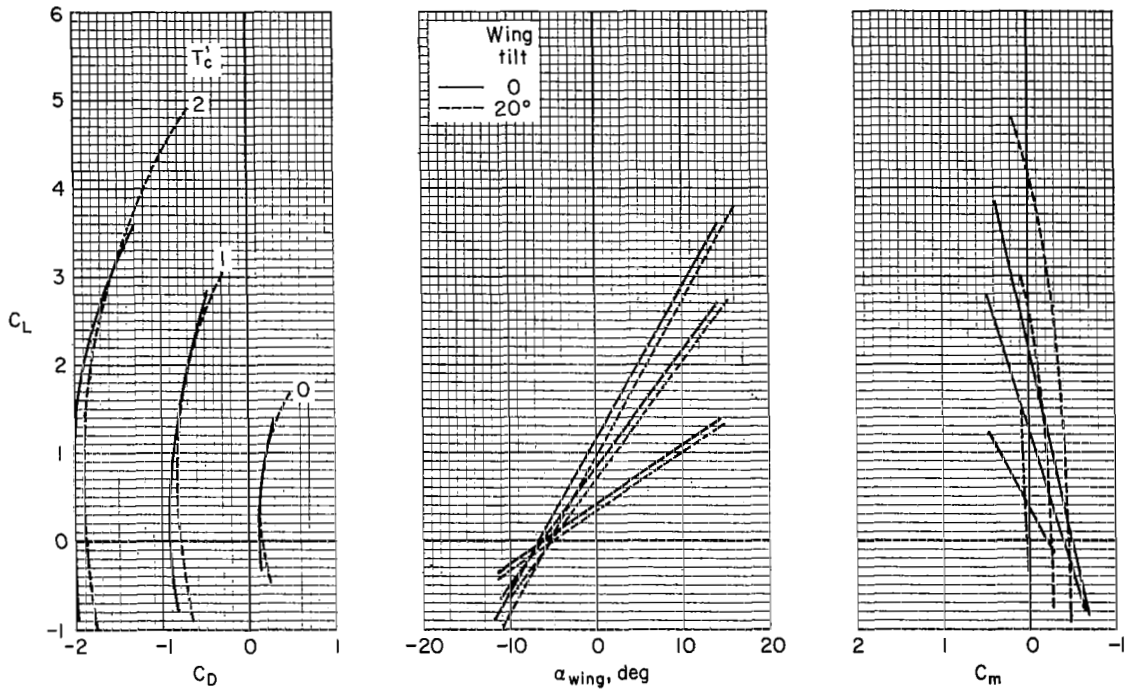

(a) $\delta_f = 0°$; $\delta_A = 0°$, $\frac{U}{V} = 0$.

Figure 11.- Effect of wing tilt; tail off, nacelle spacing B.

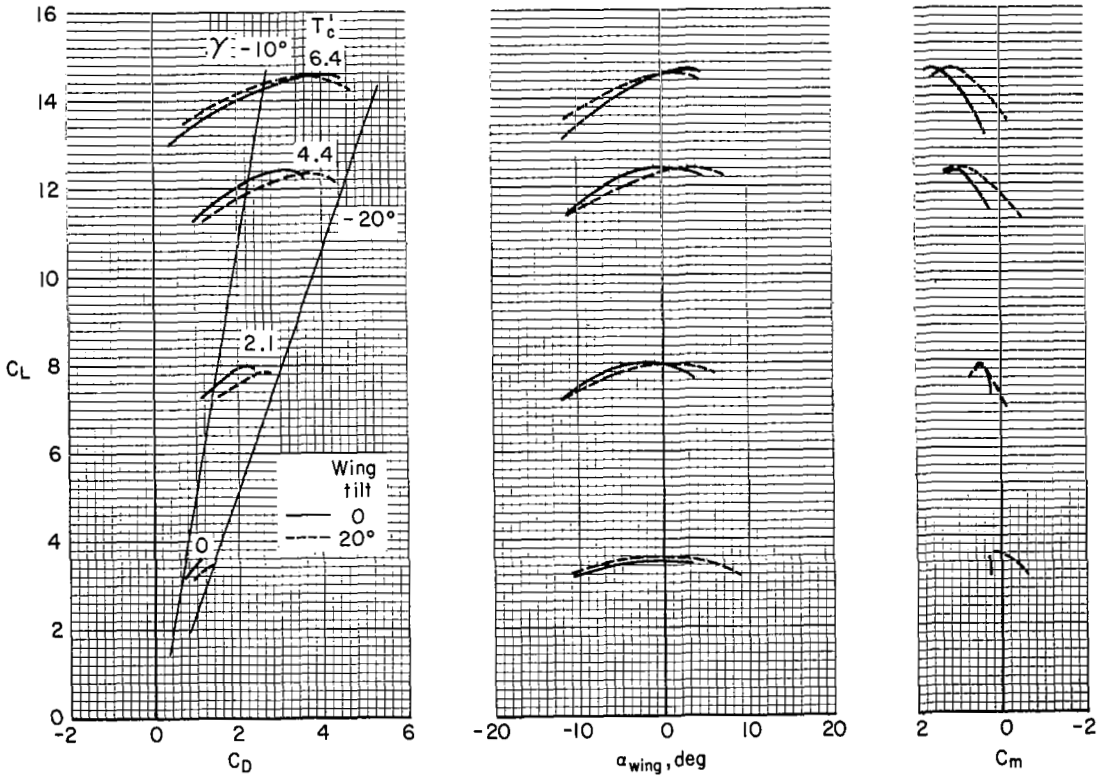

(b) $\delta_f = 70°$; $\delta_A = 20°$, $\frac{U}{V} = 6.6$

Figure 11.- Concluded.

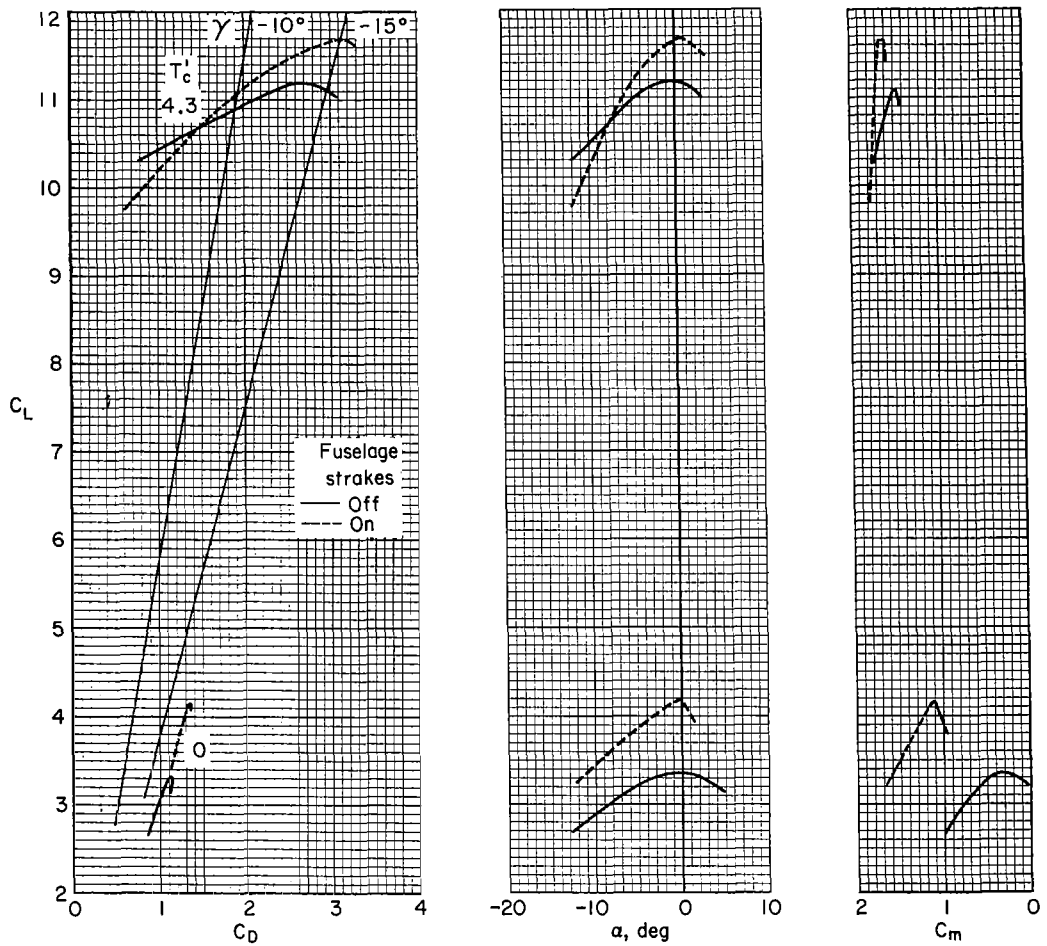

Figure 12.- Effect of fuselage strakes; δ_f = 70°, δ_A = 20°, $\frac{U}{V}$ = 6.6, tee tail, inboard slats, nacelle spacing A.

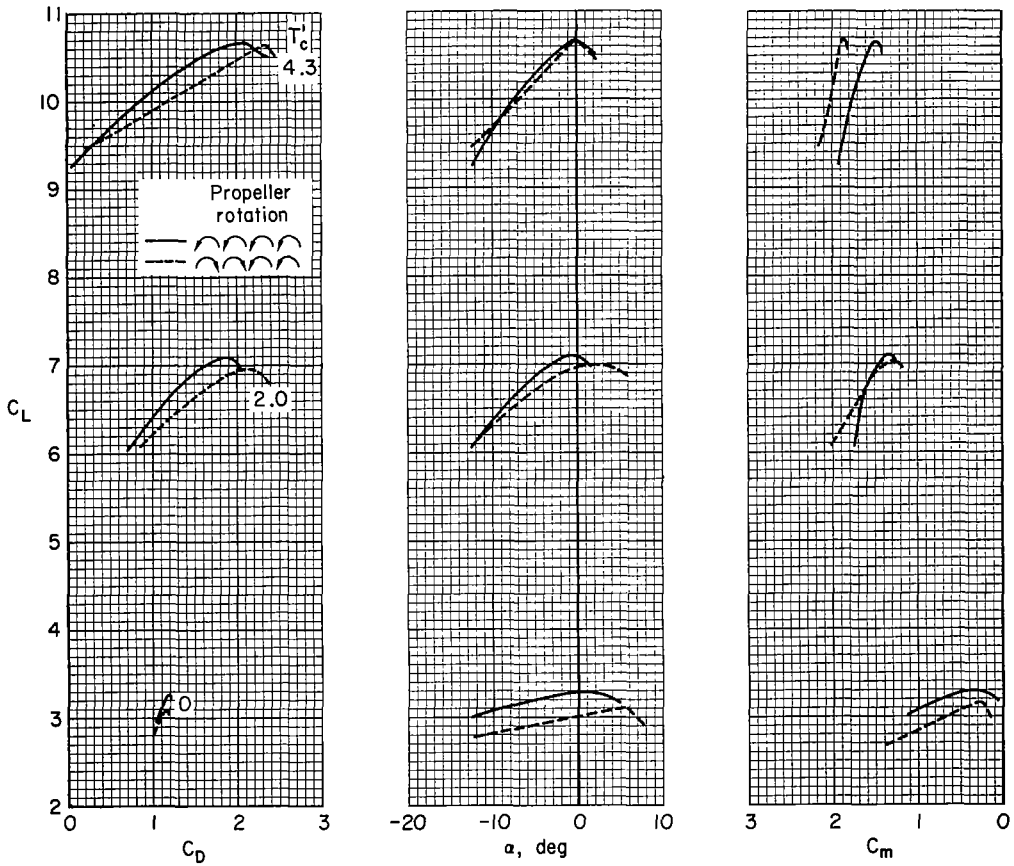

(a) C_D, α, C_m

Figure 13.- Effect of propeller rotation; $\delta_f = 80°$, $\delta_A = 0°$, $\frac{U}{V} = 6.6$, tee tail, nacelle spacing A.

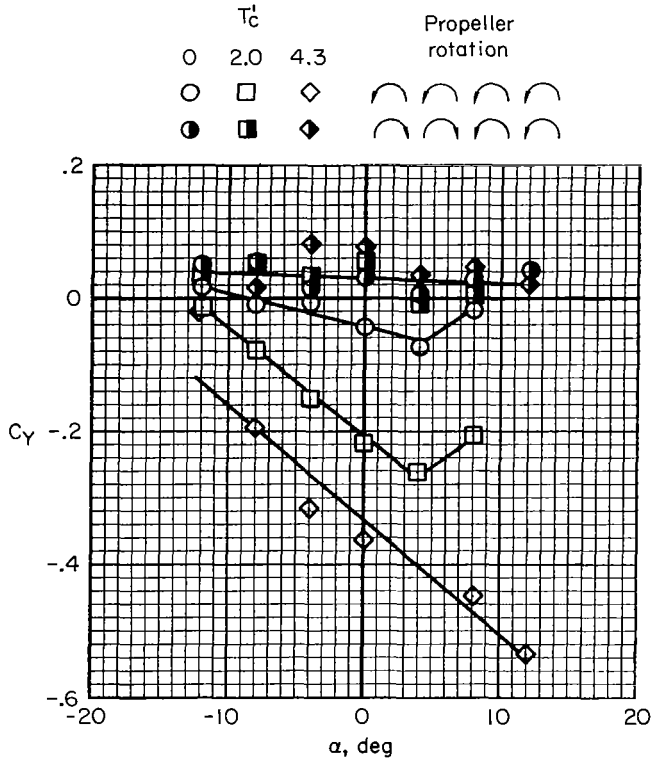

(b) C_Y

Figure 13.- Concluded.

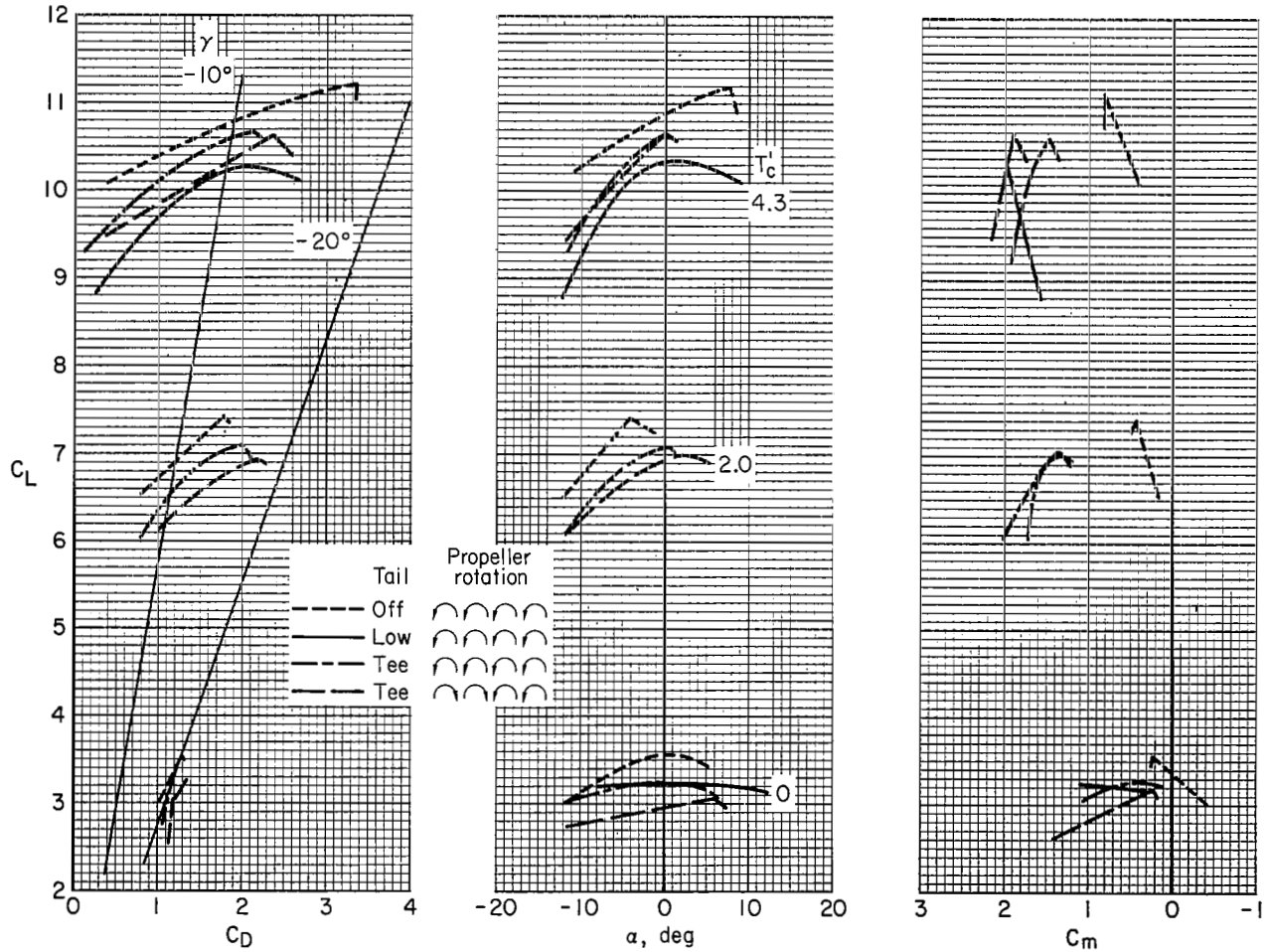

(a) $\delta_f = 80°$; $\delta_A = 0°$, $\frac{U}{V} = 6.6$

Figure 14.- Effect of a horizontal tail; nacelle spacing A.

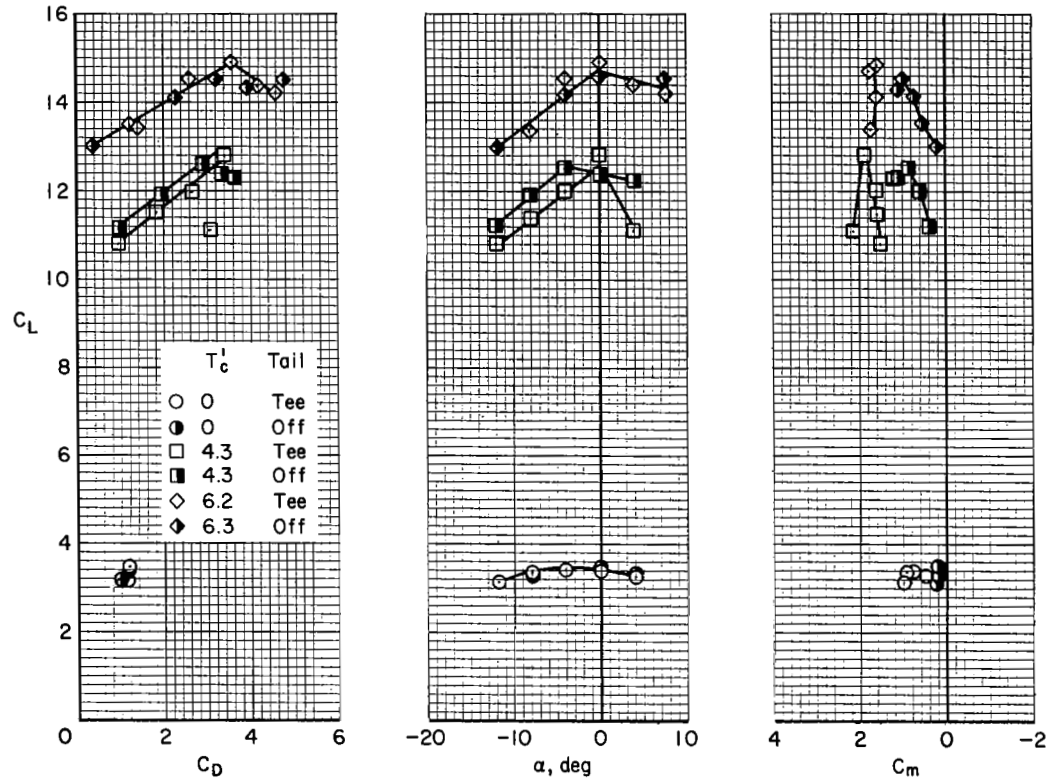

(b) $\delta_f = 70°$; $\delta_A = 20°$, $\frac{U}{V} = 6.6$

Figure 14.- Concluded.

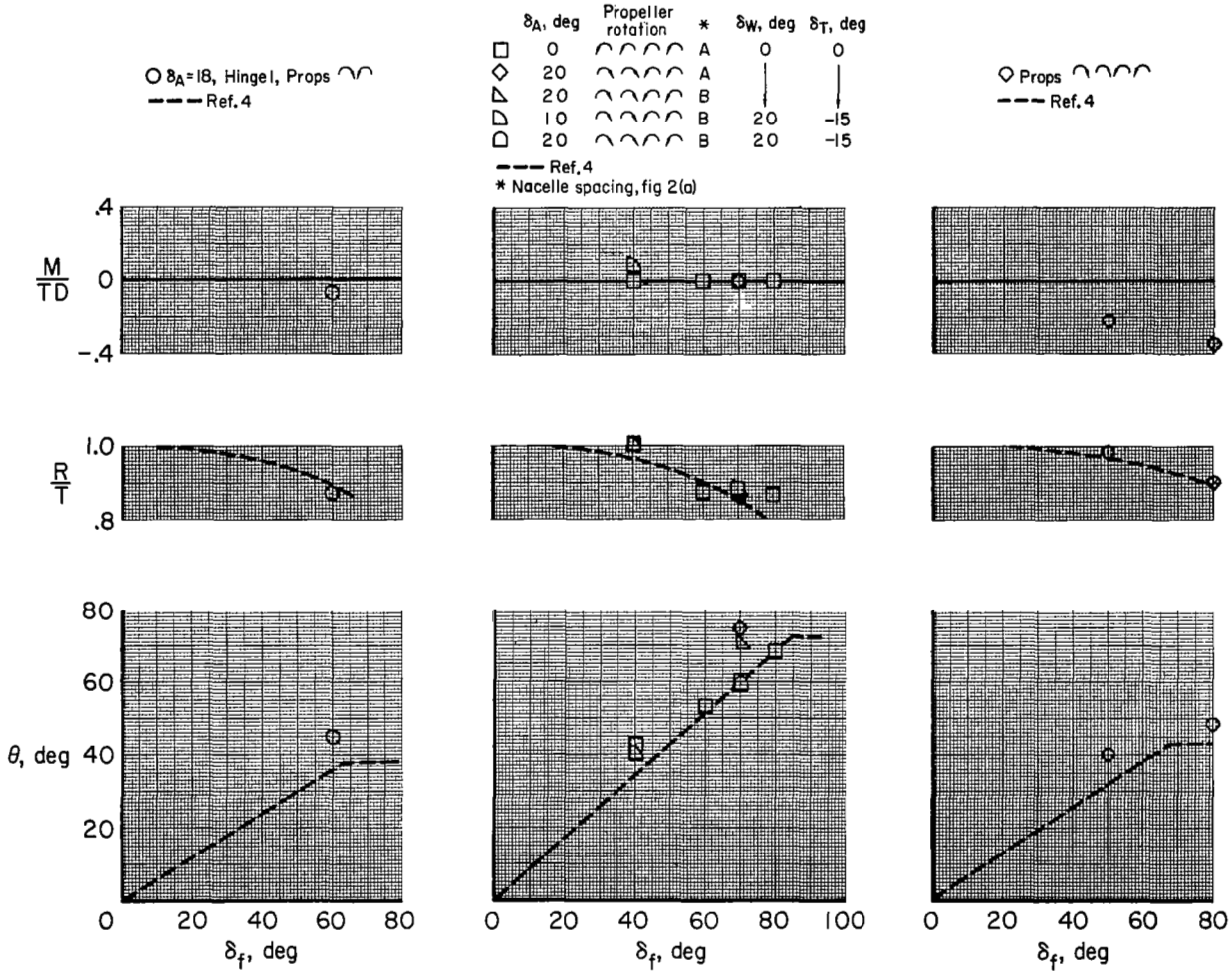

Figure 15.- Zero airspeed characteristics.

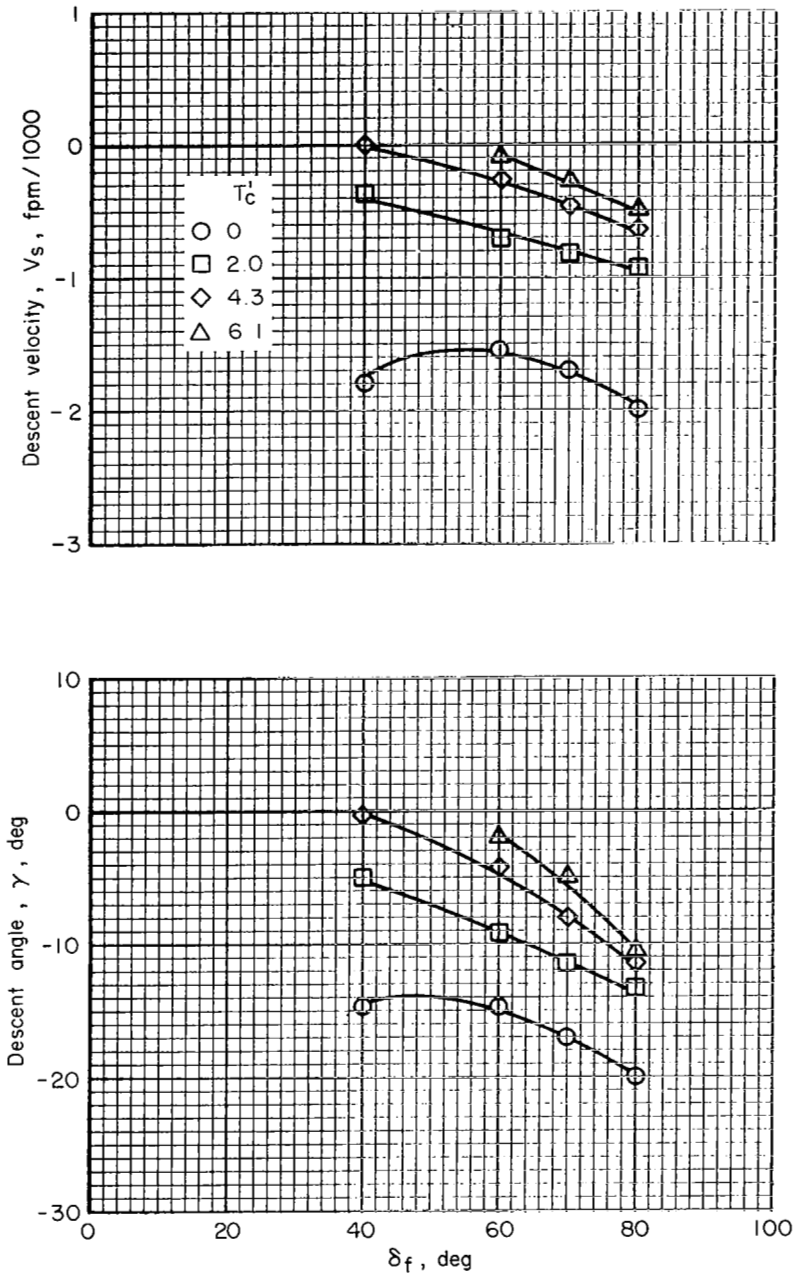

(a) Effect of flap deflection; $\delta_A = 0°$.

Figure 16.- Descent characteristics.

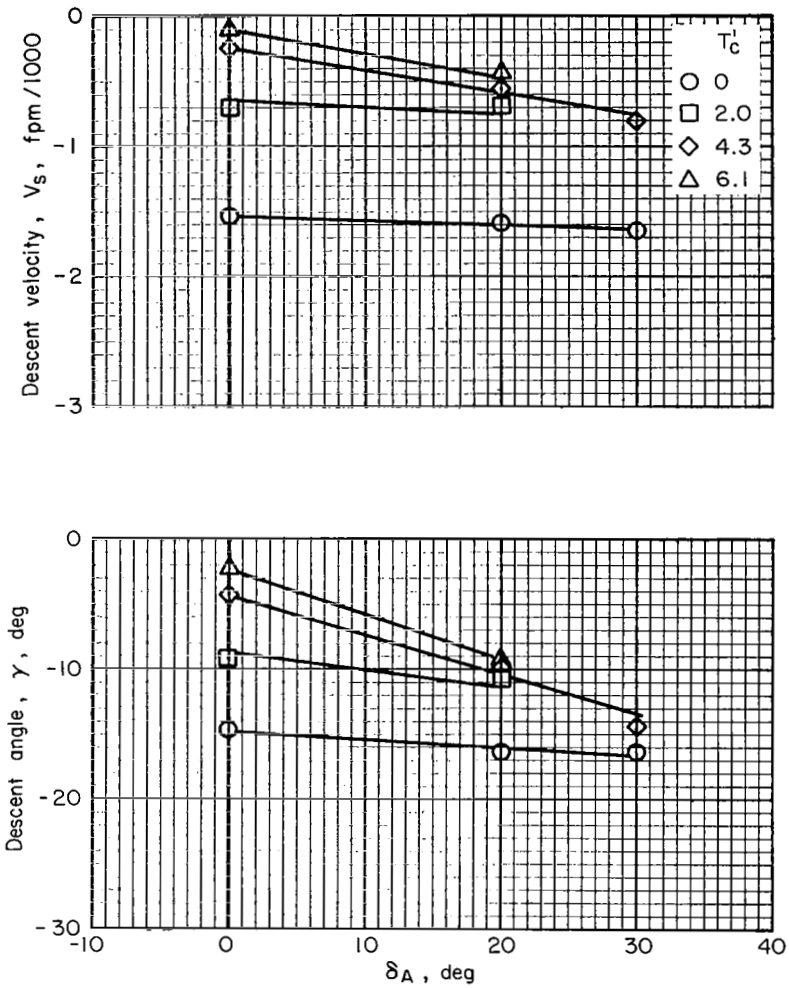

(b) Effect of aft flap; $\delta_f = 60°$.

Figure 16.- Continued.

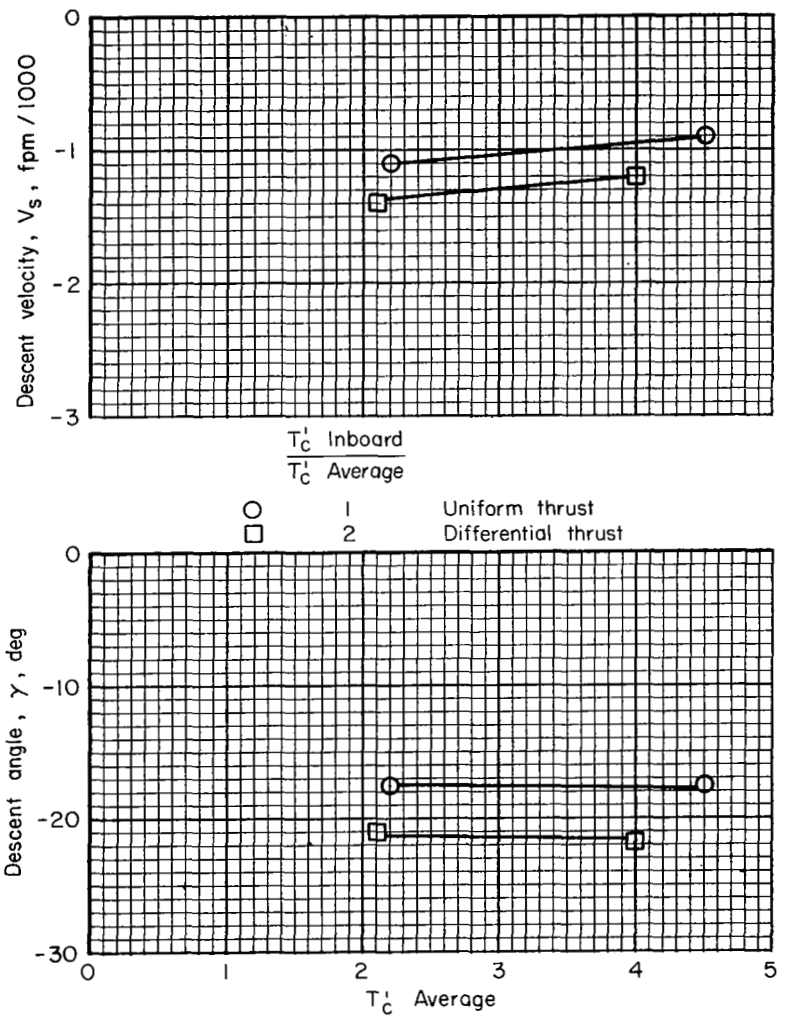

(c) Effect of differential thrust; $\delta_f = 70°$, $\delta_A = 20°$.

Figure 16.- Concluded.

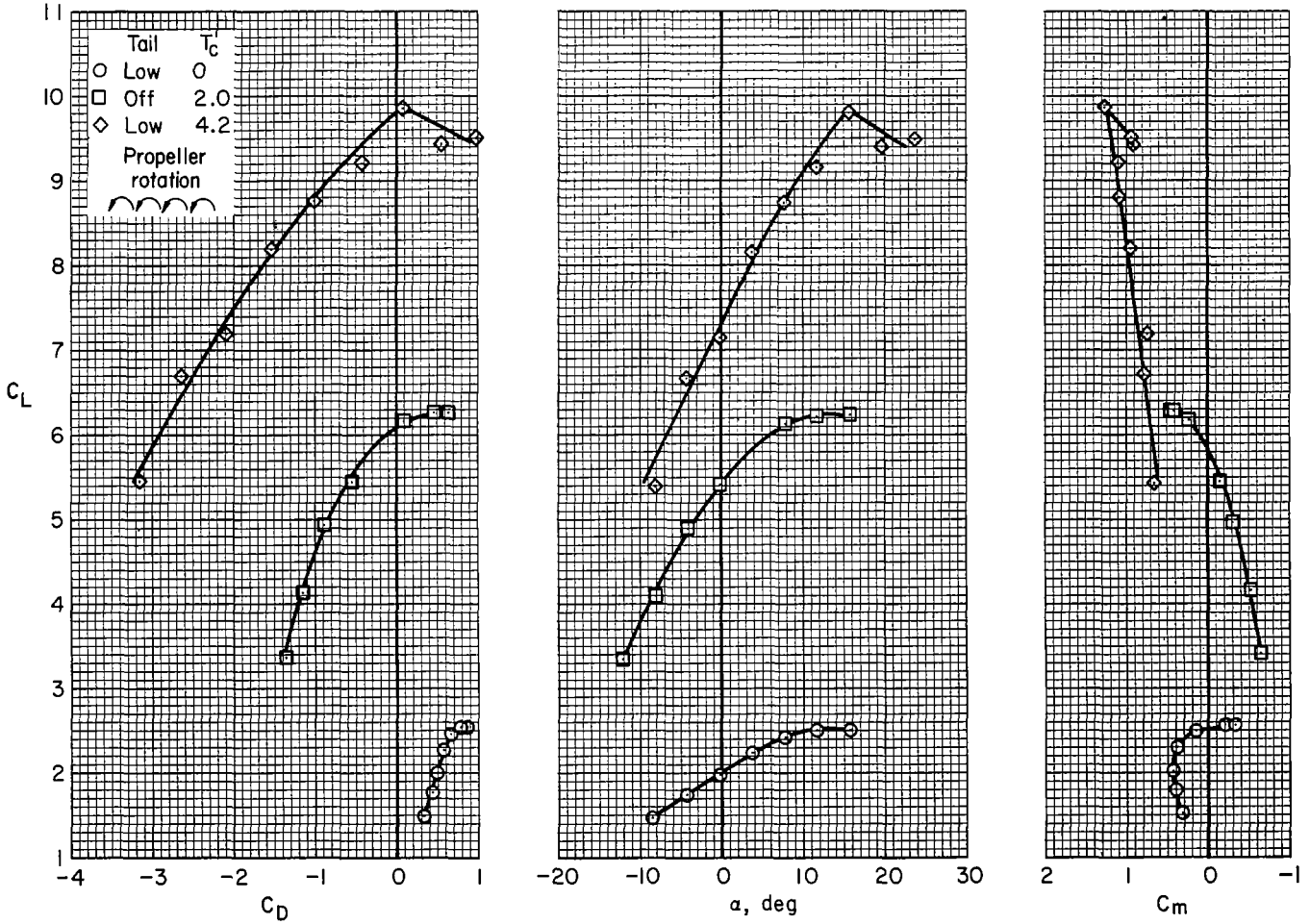

(a) $\delta_A = 0°$, $\frac{U}{V} = 5.0$

Figure 17.- Aerodynamic characteristics; $\delta_f = 40°$, nacelle spacing A.

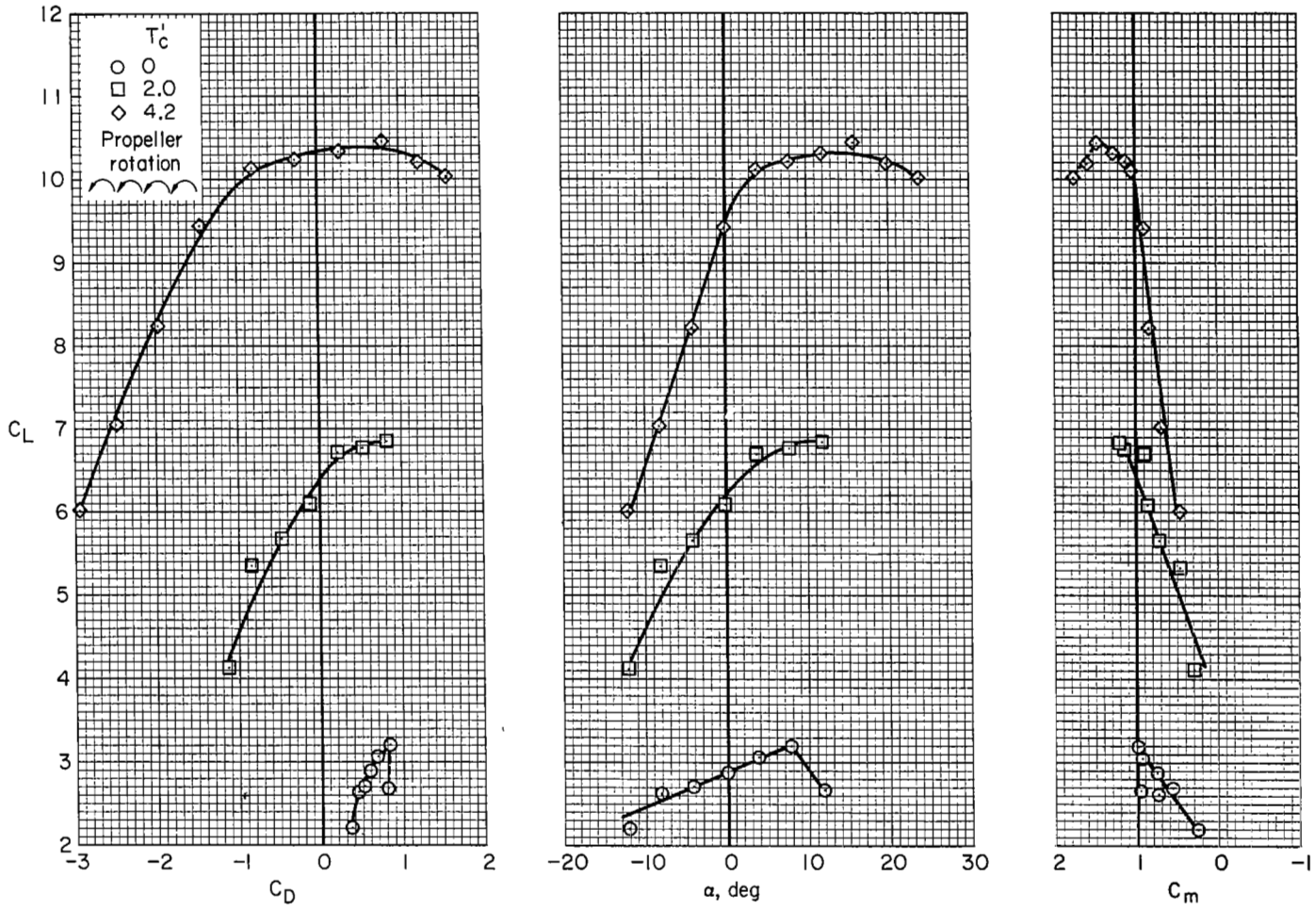

(b) $\delta_A = 10°$; $\frac{U}{V} = 6.6$, tail off.

Figure 17.- Continued.

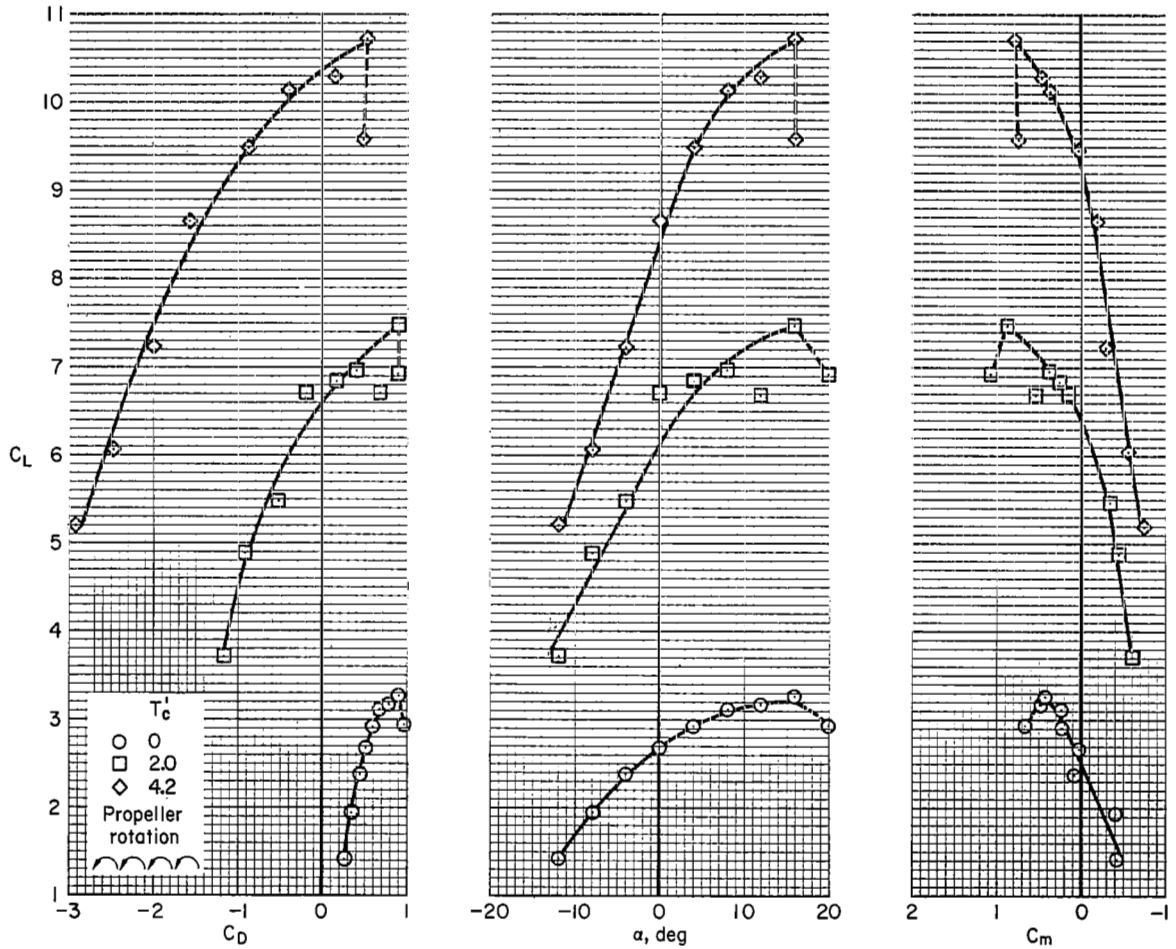

(c) $\delta_A = 10°$; $\frac{U}{V} = 6.6$, slats on, tail off.

Figure 17.- Concluded.

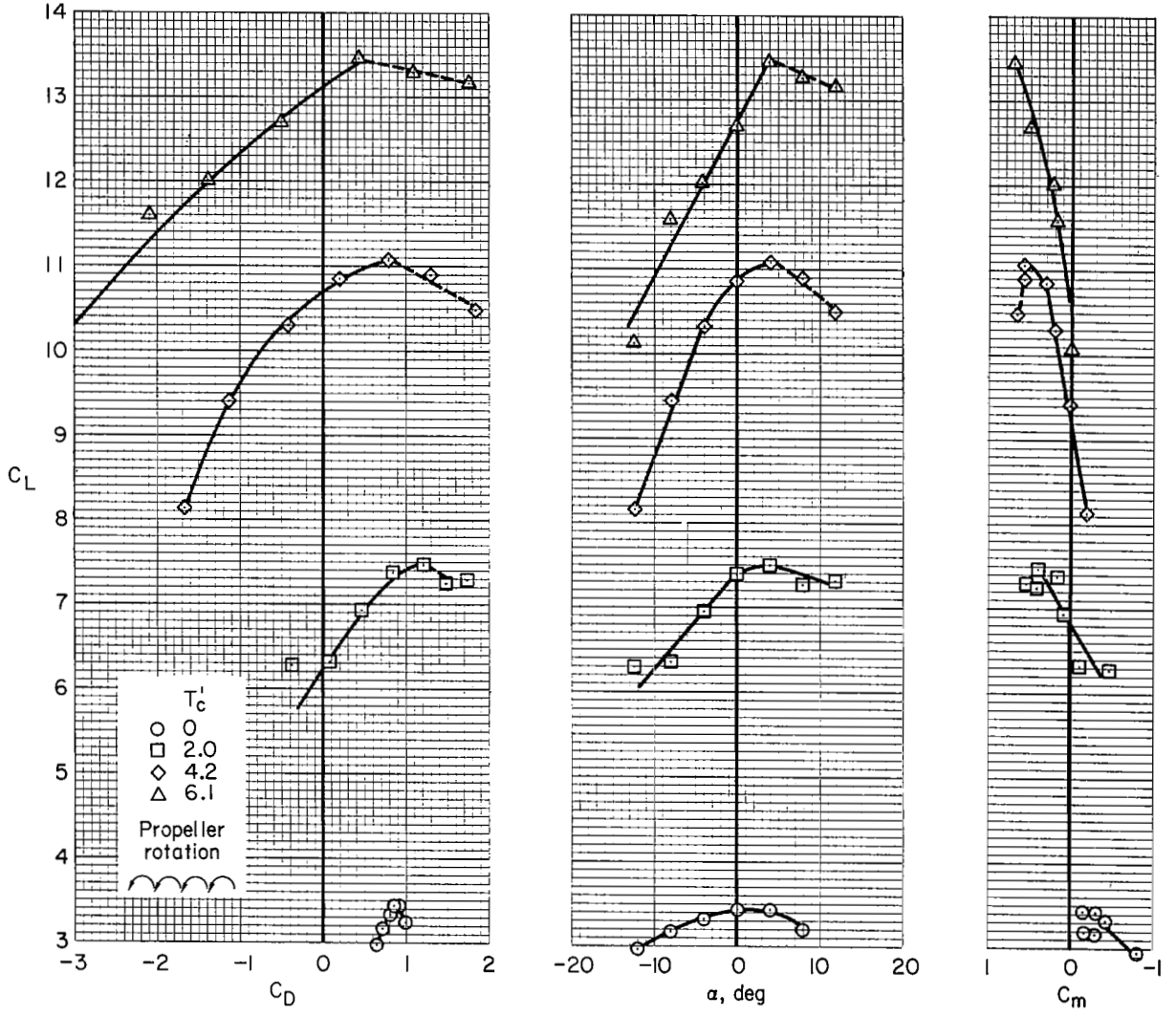

(a) $\delta_A = 0°$; tail off.

Figure 18.- Aerodynamic characteristics; $\delta_f = 60°$, $\frac{U}{V} = 6.6$, nacelle spacing A.

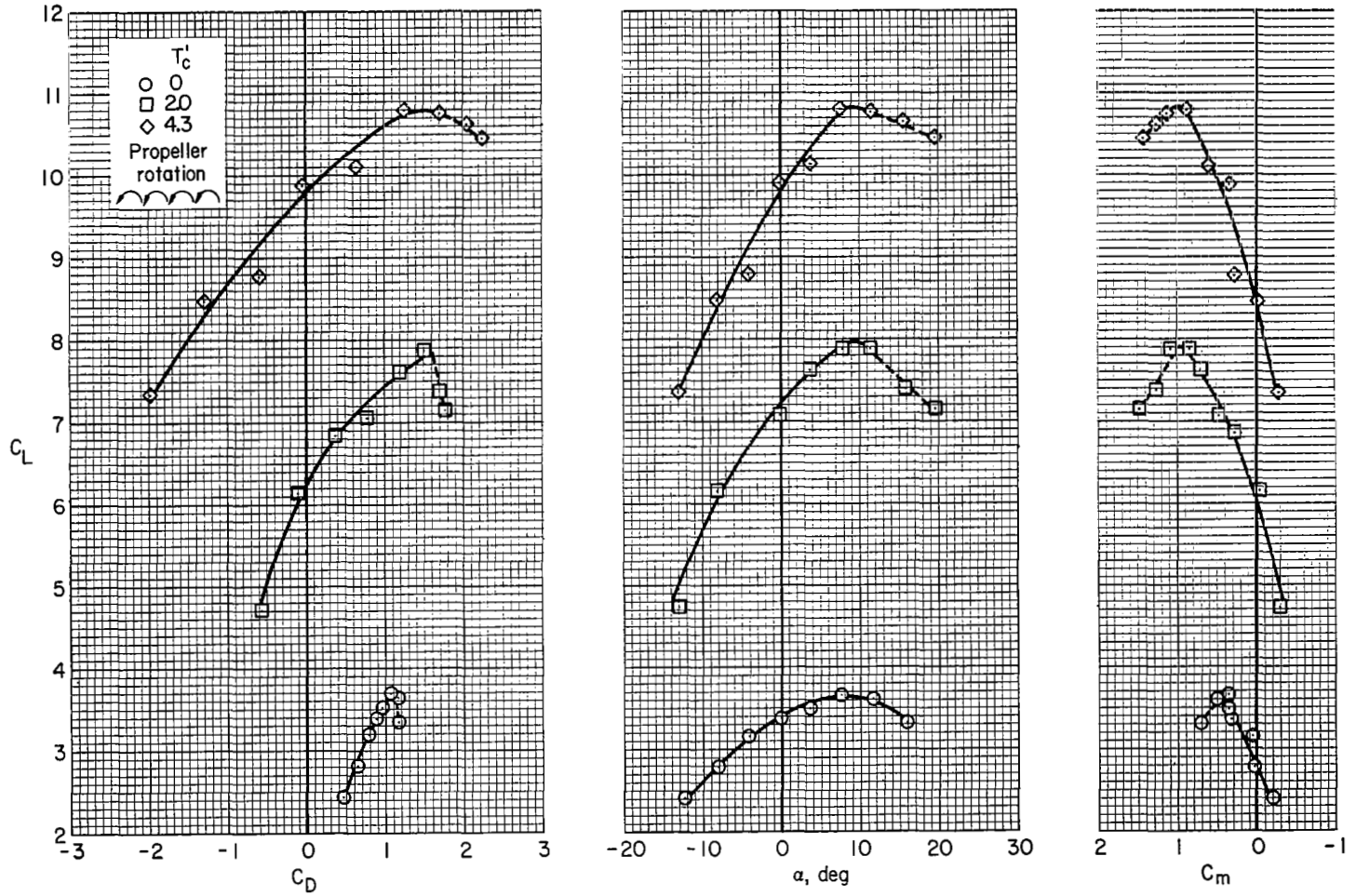

(b) $\delta_A = 0°$; tail off, slats on.

Figure 18.- Continued.

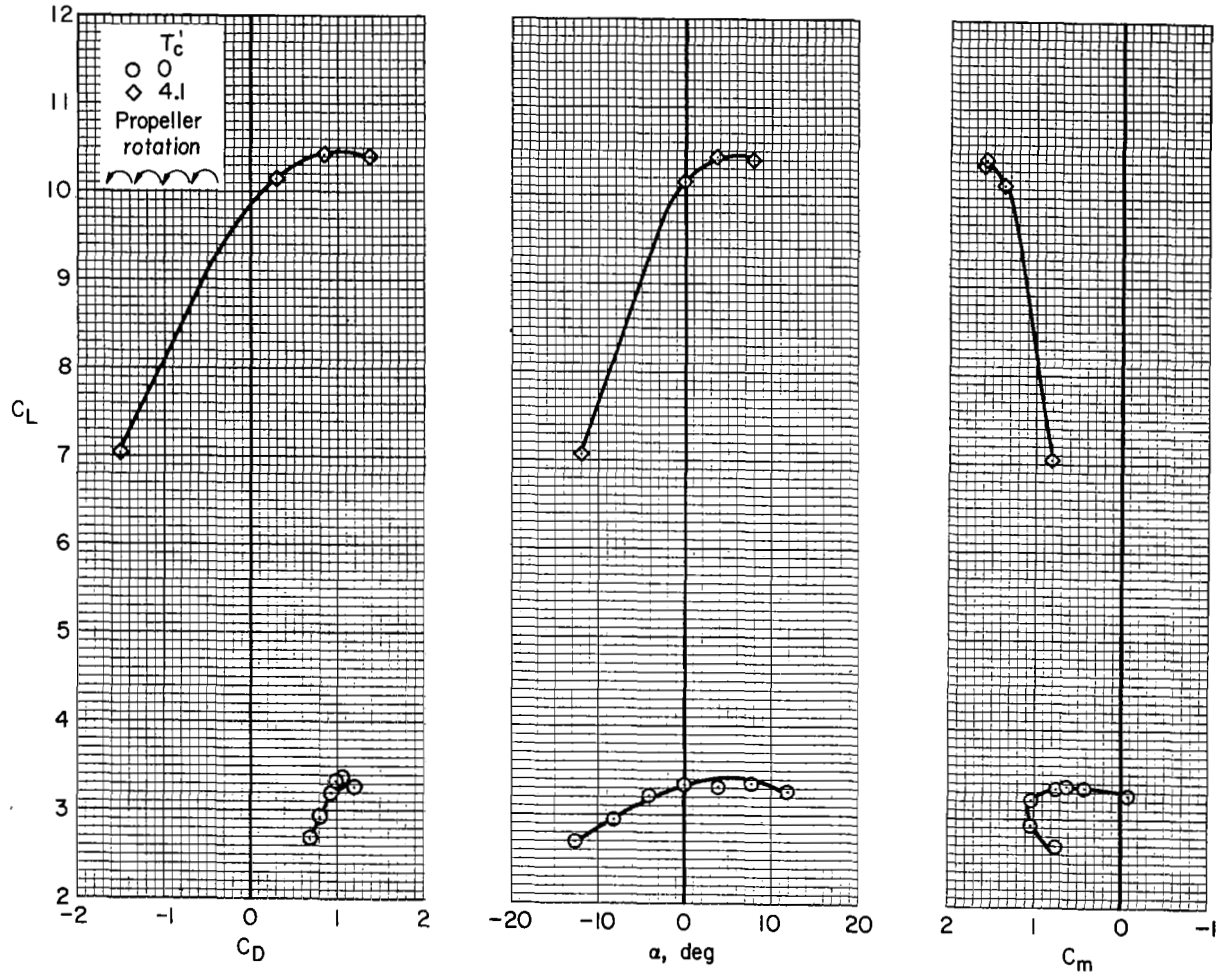

(c) $\delta_A = 0°$; low tail.

Figure 18.- Continued.

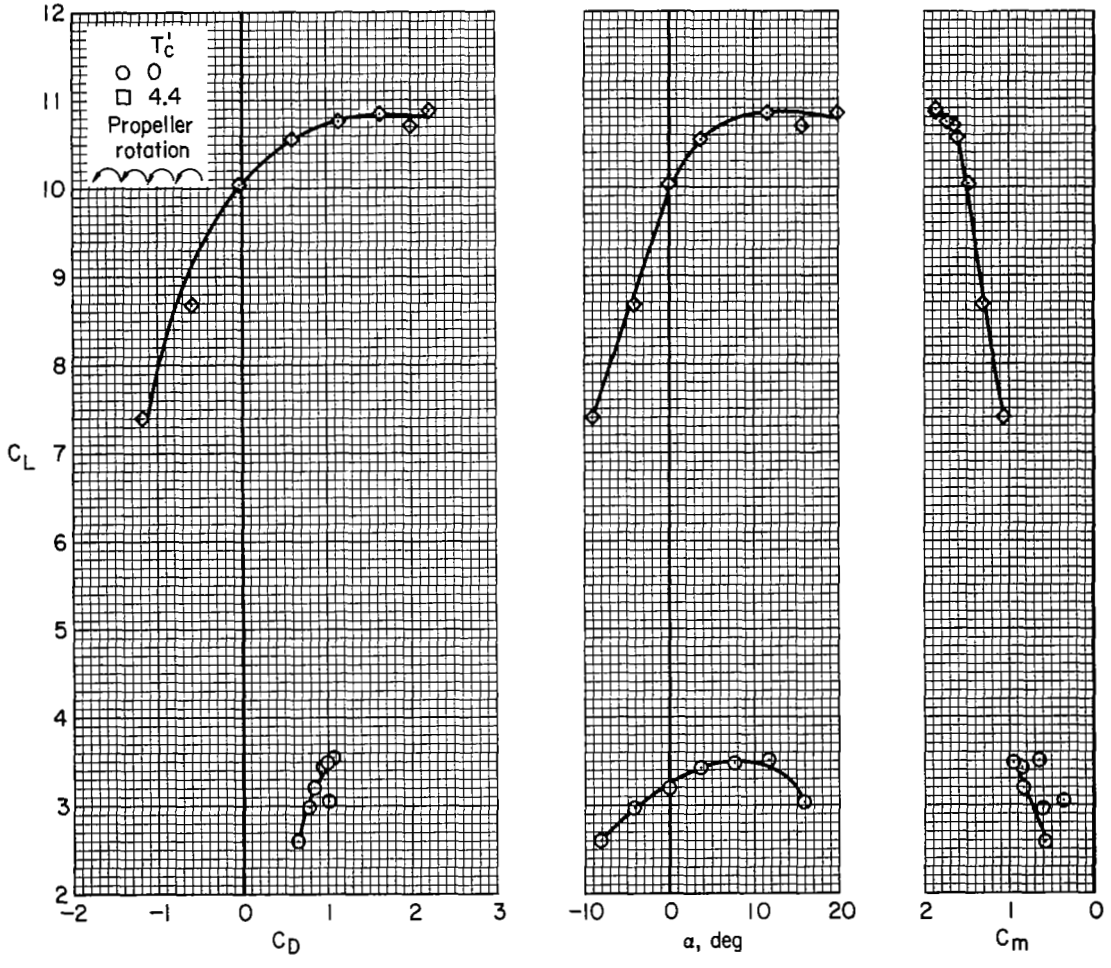

(d) $\delta_A = 0°$; low tail, slats on.

Figure 18.- Continued.

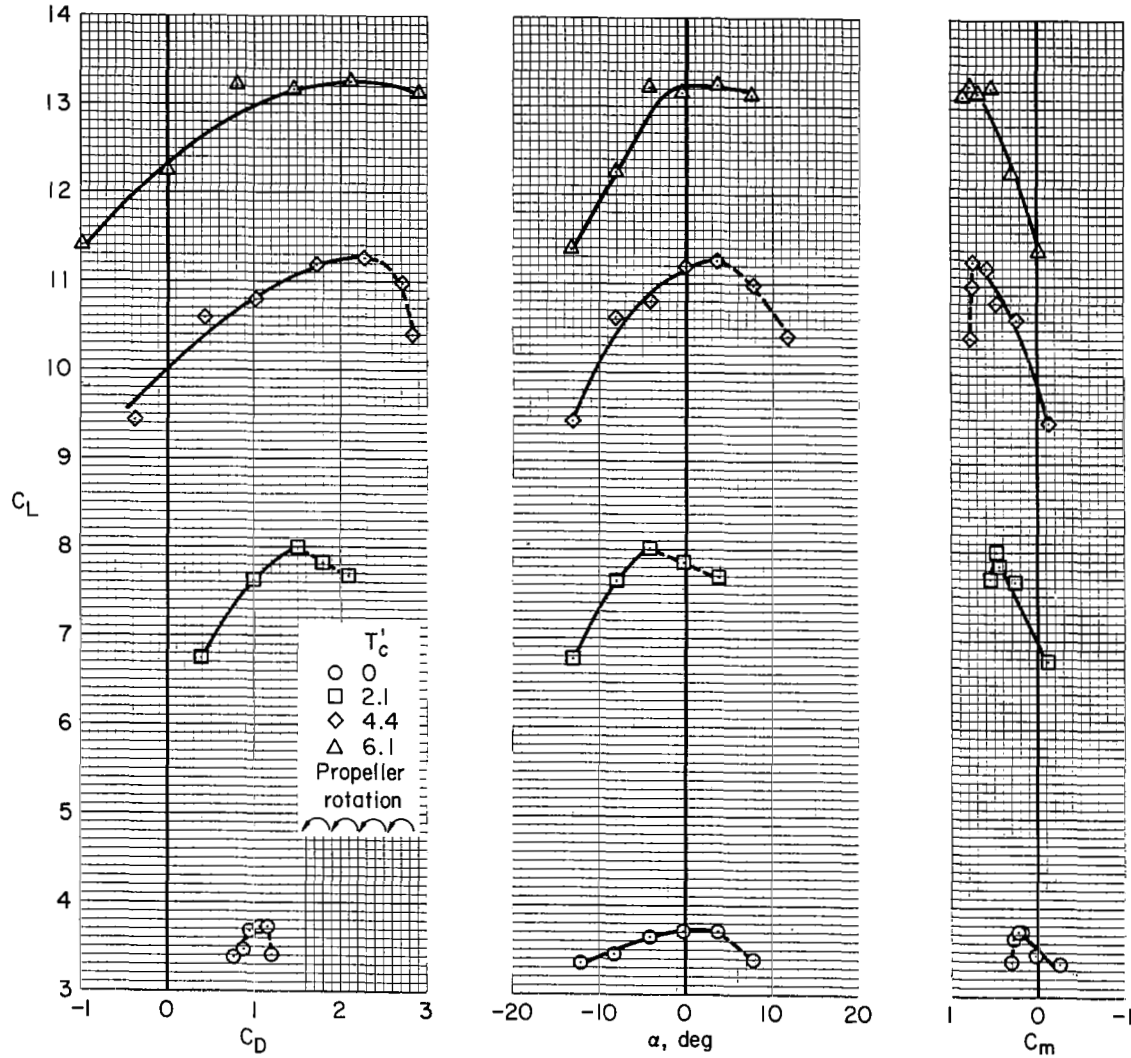

(e) $\delta_A = 20°$; tail off.

Figure 18.- Continued.

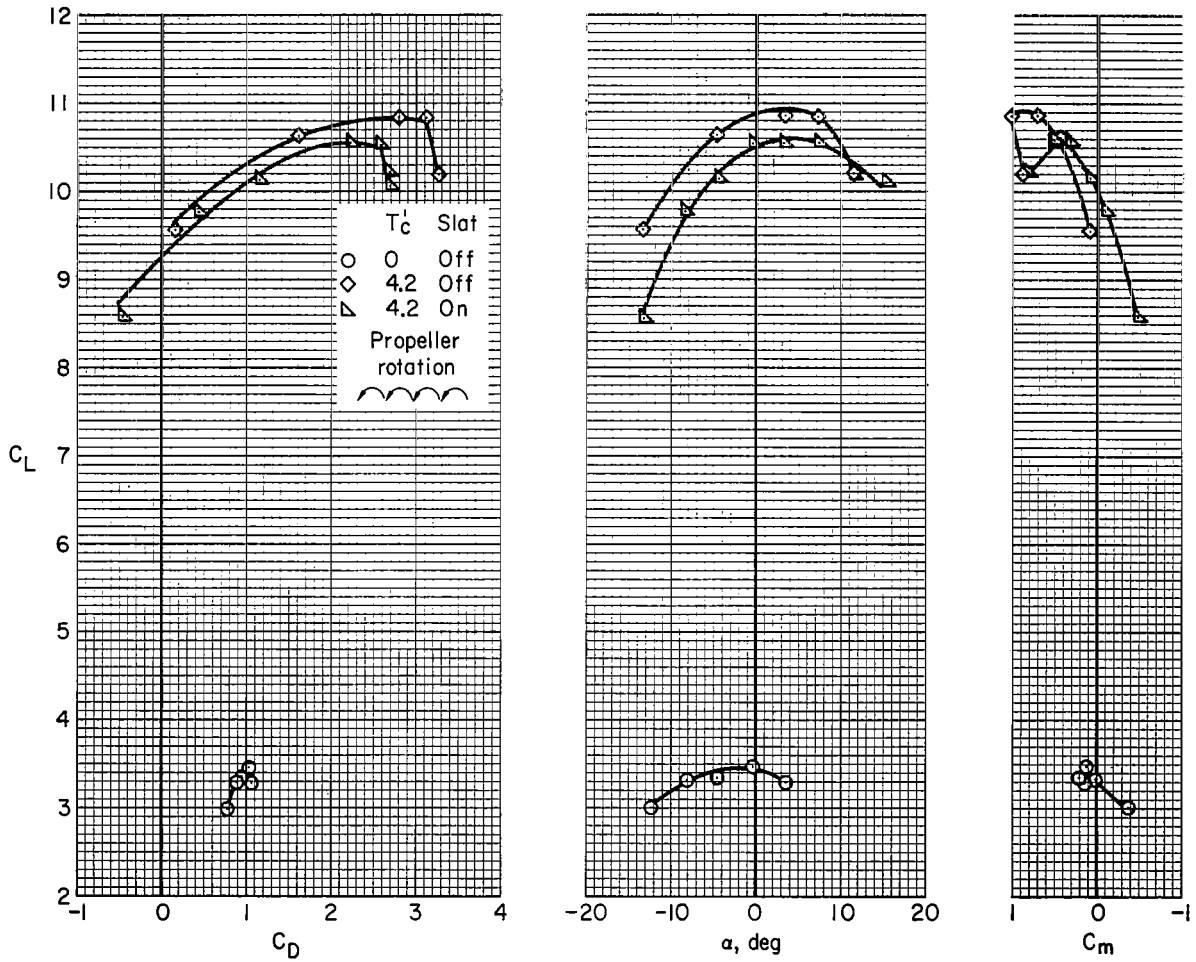

(f) δ_A = 30°; tail off.

Figure 18.- Continued.

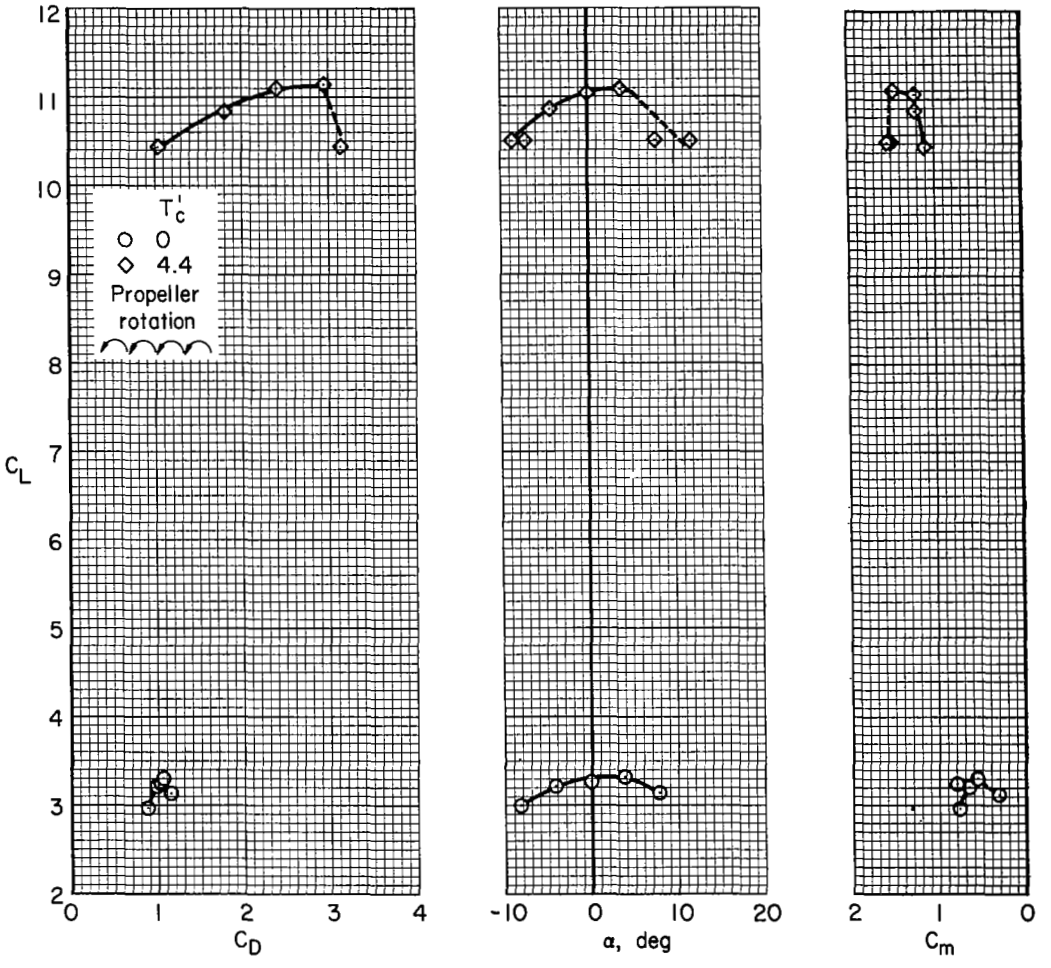

(g) $\delta_A = 30°$; low tail.

Figure 18.- Concluded.

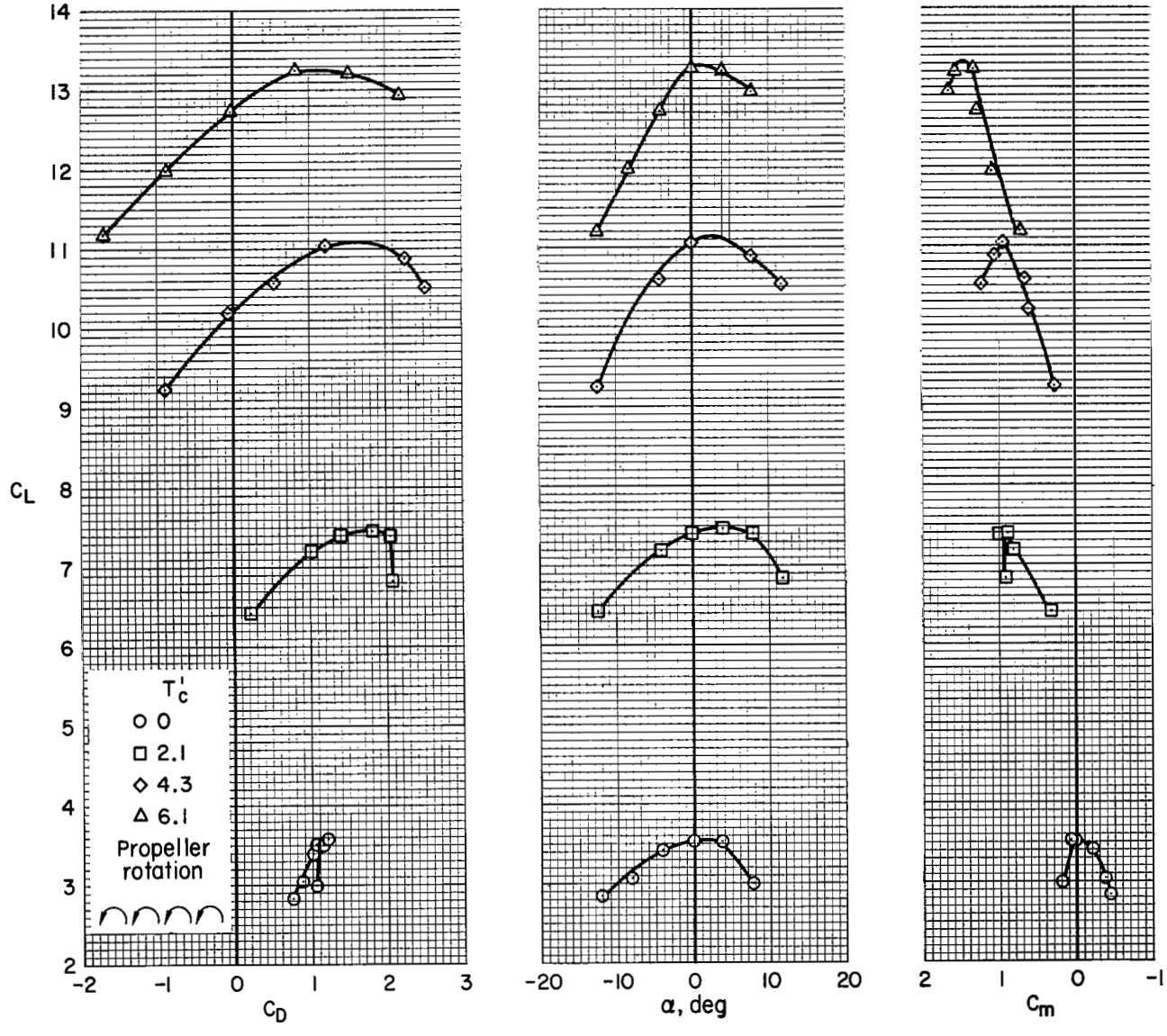

(a) $\delta_A = 0°$; tail off.

Figure 19.- Aerodynamic characteristics; $\delta_f = 70°$, $\frac{U}{V} = 6.6$, nacelle spacing A.

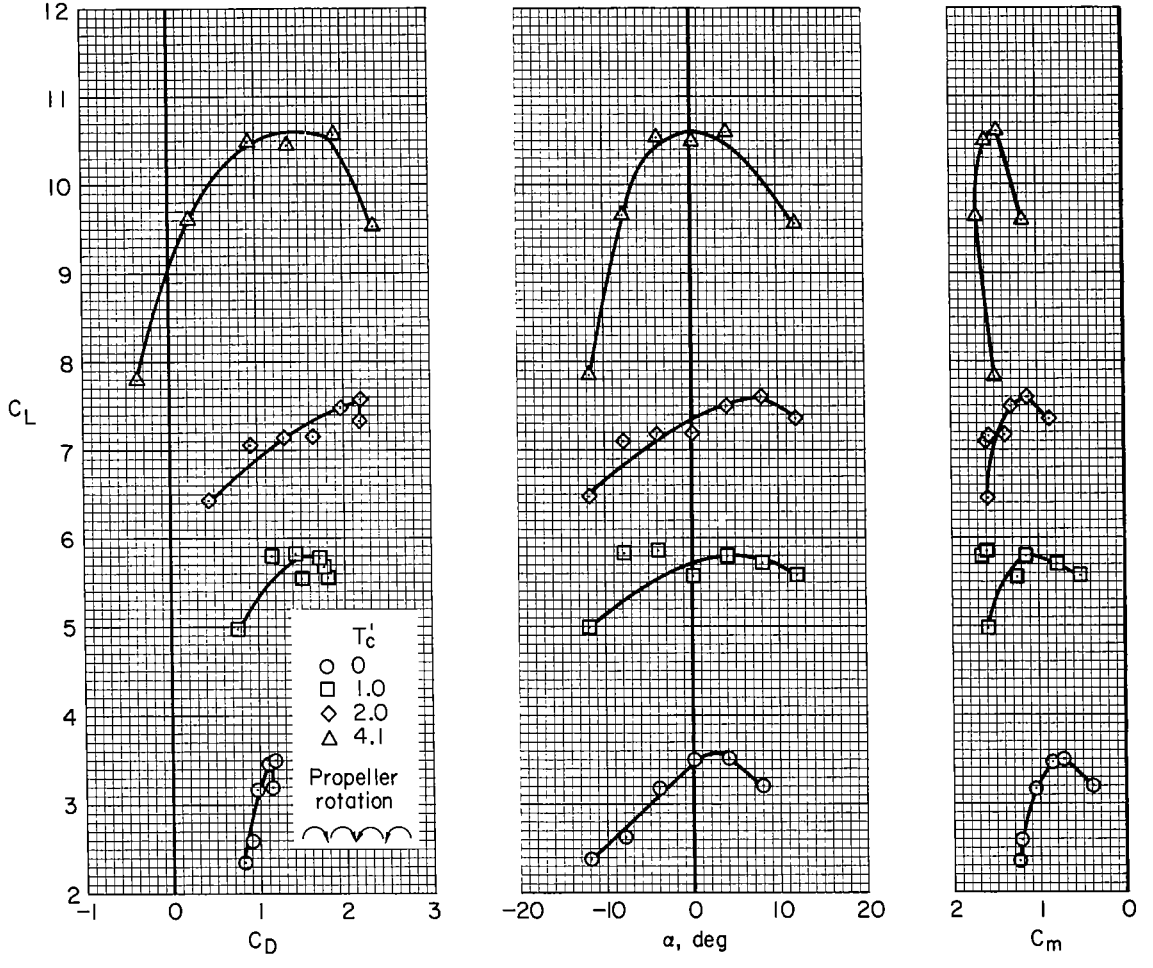

(b) $\delta_A = 0°$; tee tail.

Figure 19.- Continued.

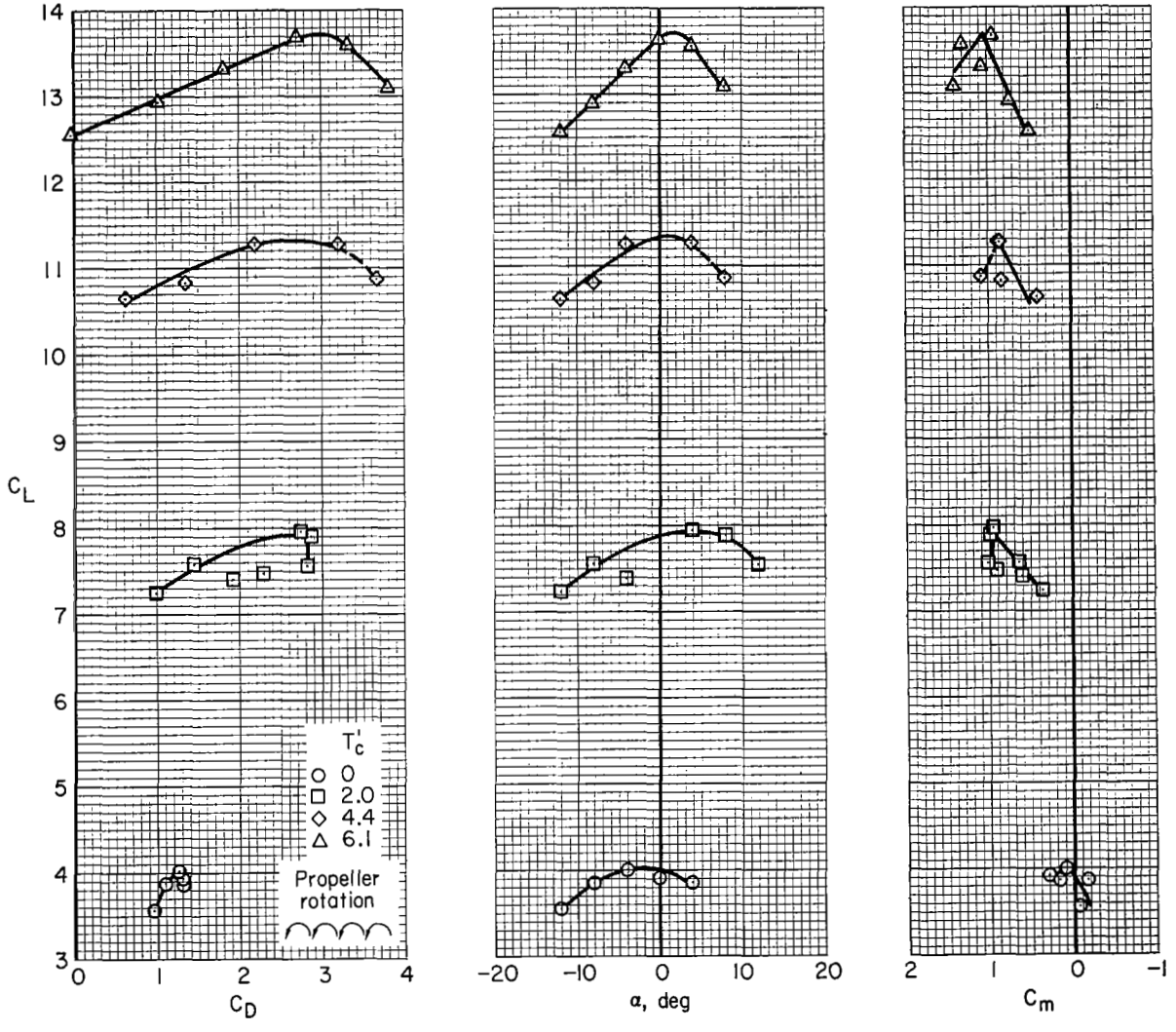

(c) $\delta_A = 20°$; tail off.

Figure 19.- Continued.

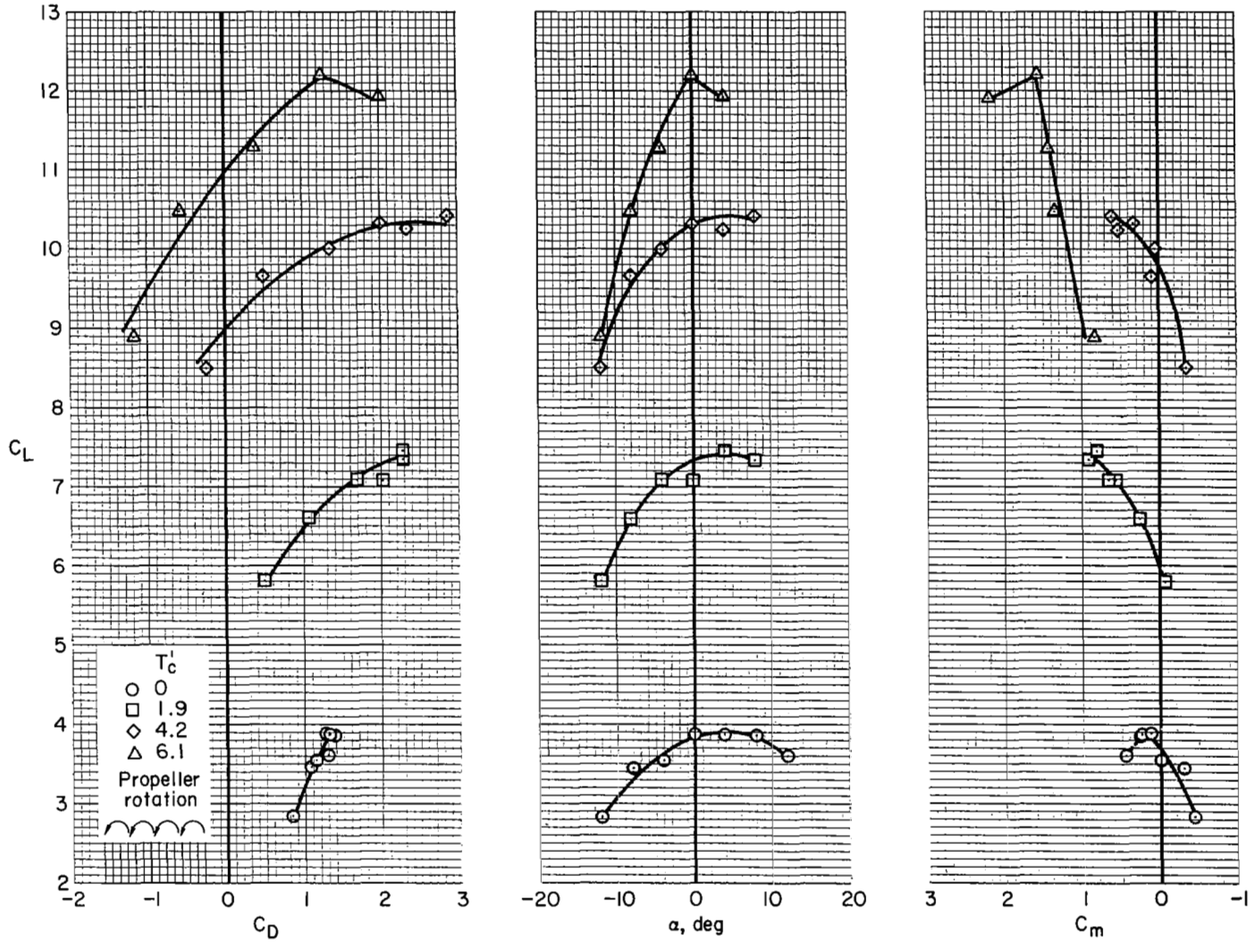

(d) δ_A = 20°; tail off, slats on.

Figure 19.- Continued.

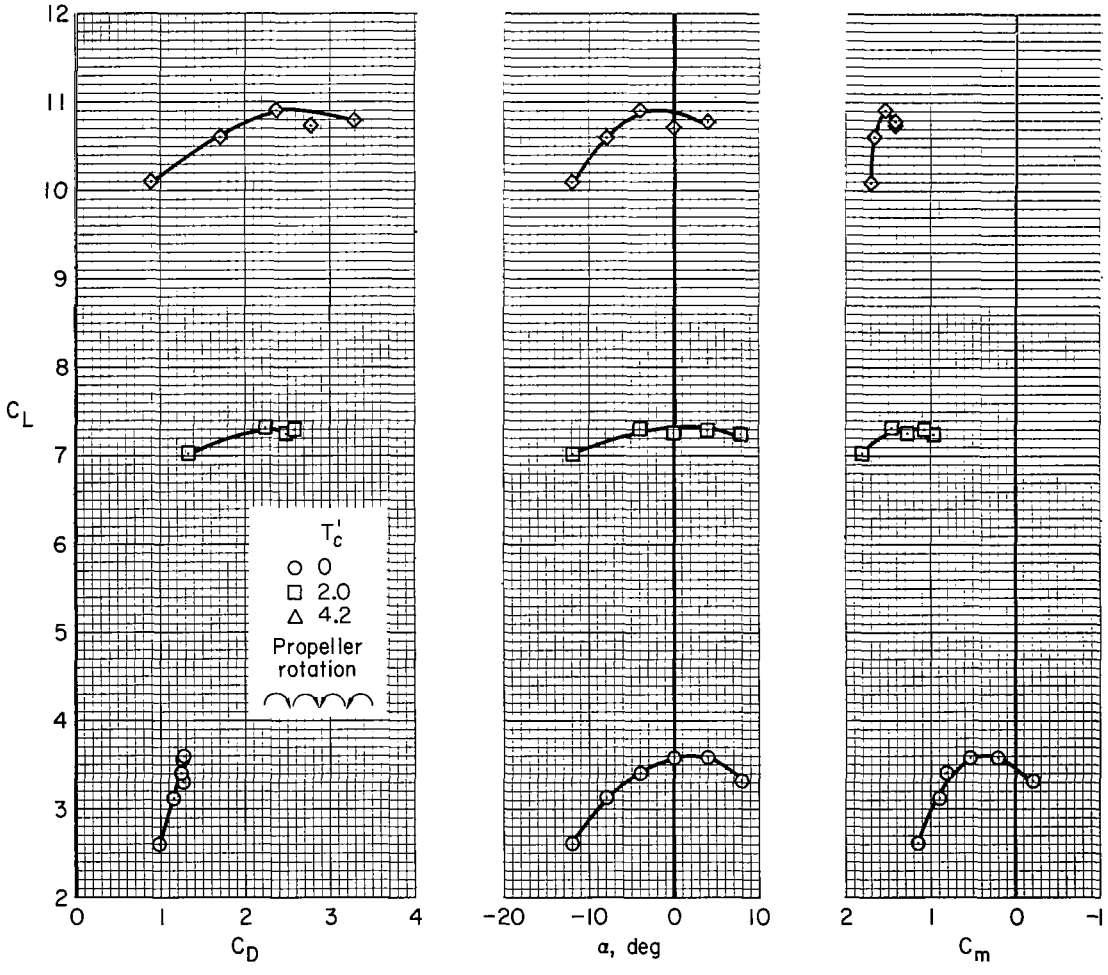

(e) $\delta_A = 20°$; tee tail.

Figure 19.- Concluded.

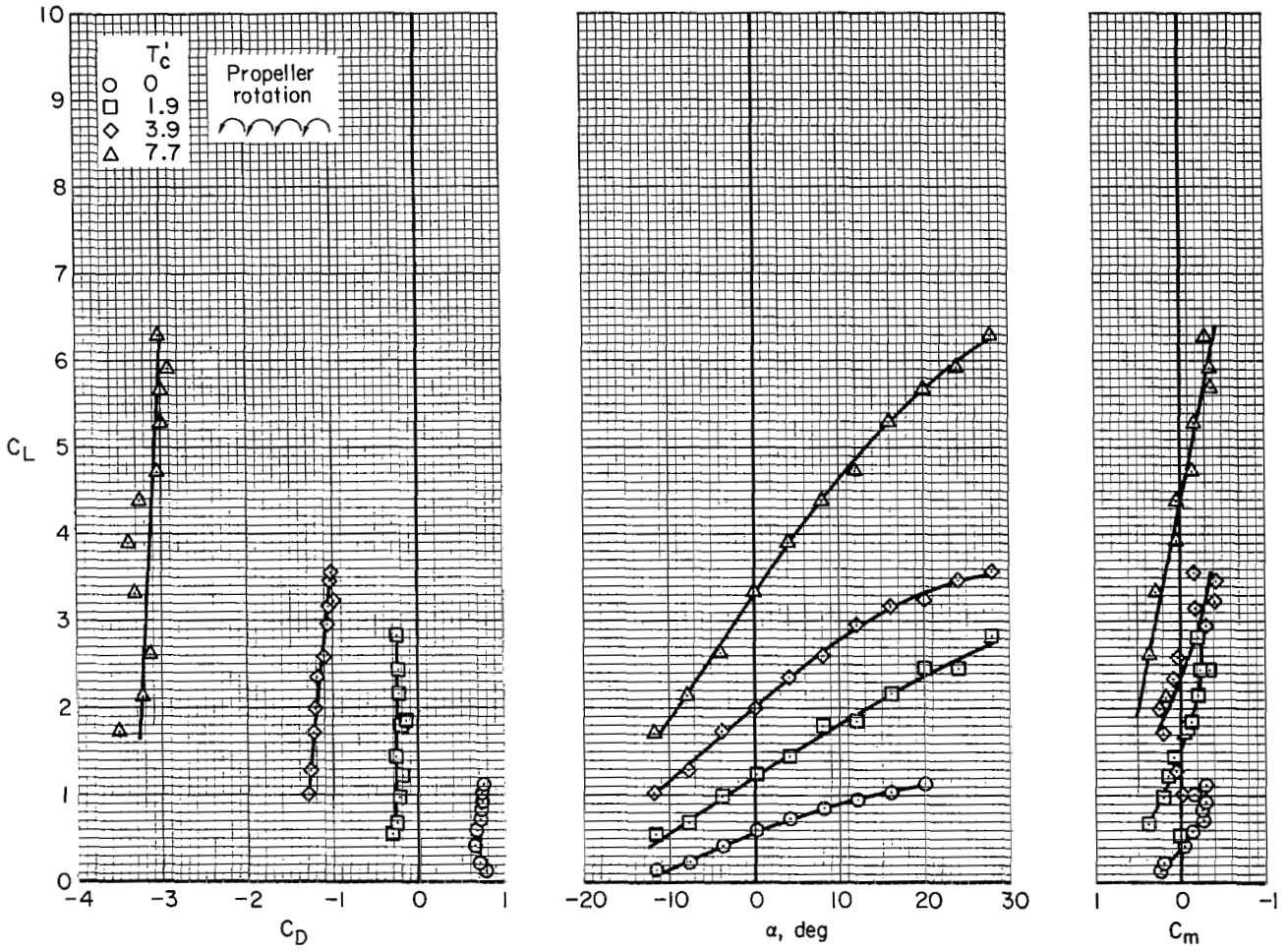

(a) $\frac{U}{V} = 0$; low tail.

Figure 20.- Aerodynamic characteristics; $\delta_f = 80°$, $\delta_A = 0°$, nacelle spacing A.

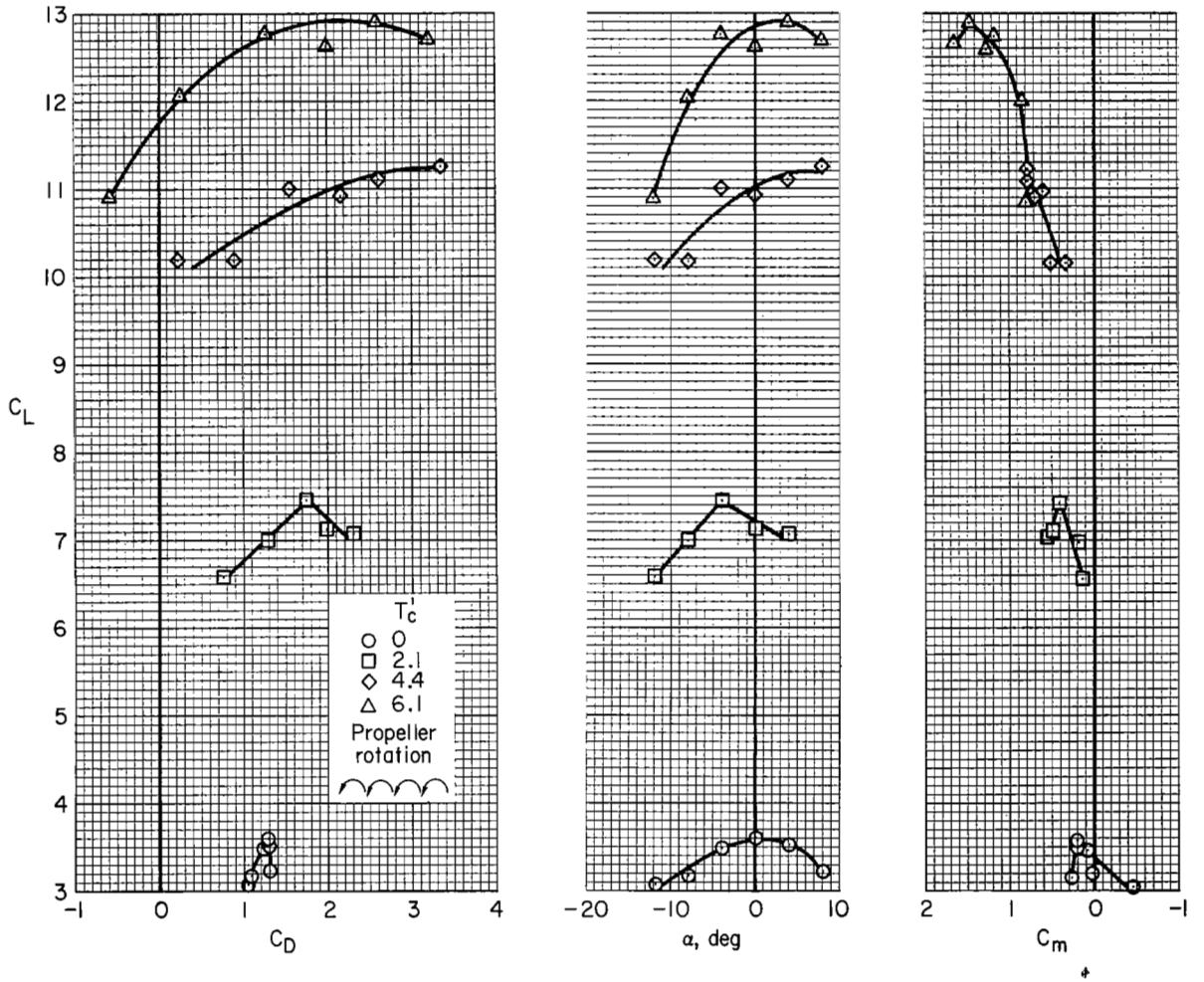

(b) $\frac{U}{V}$ = 6.6; tail off.

Figure 20.- Continued.

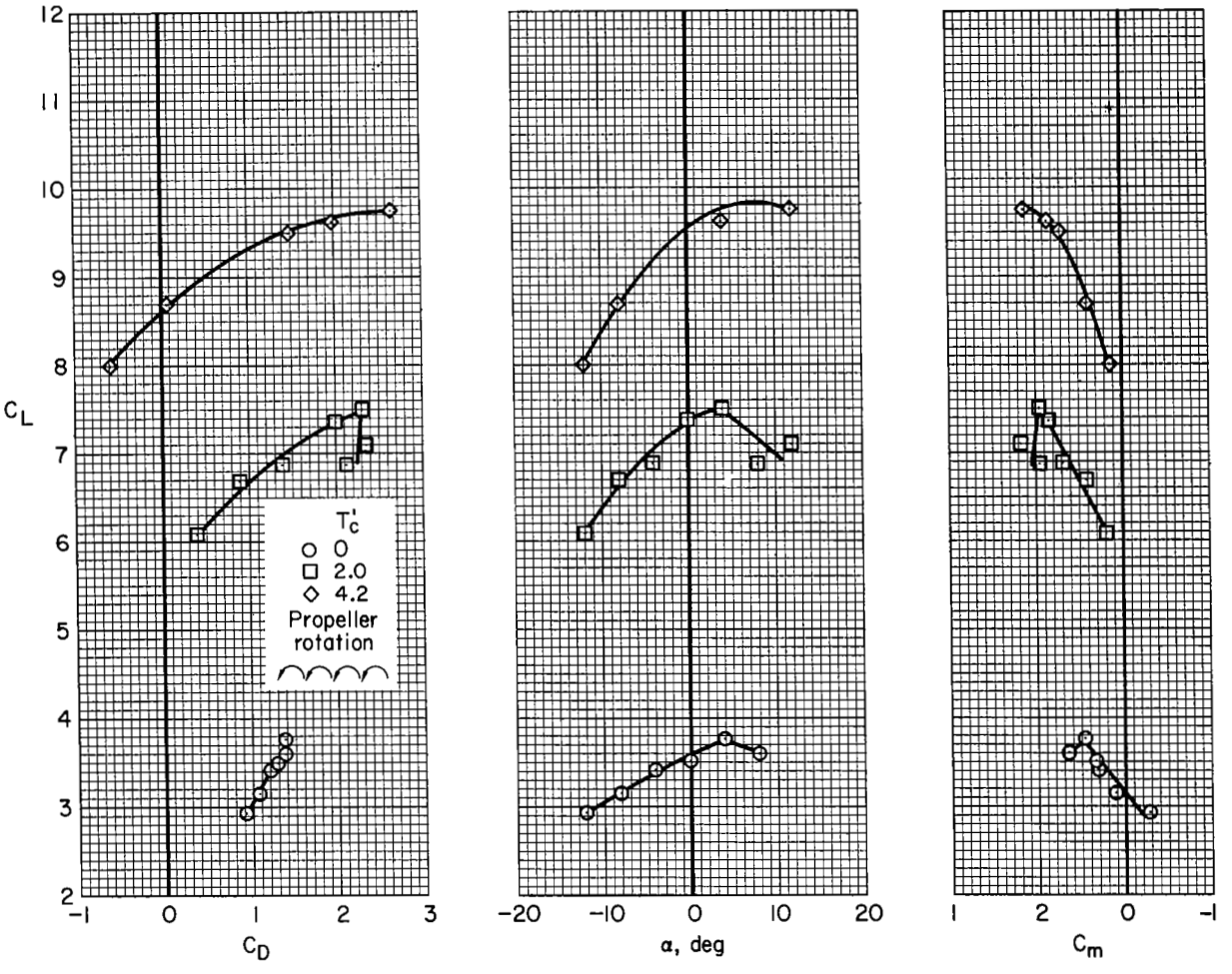

(c) $\frac{U}{V}$ = 6.6; tail off, slats on.

Figure 20.- Continued.

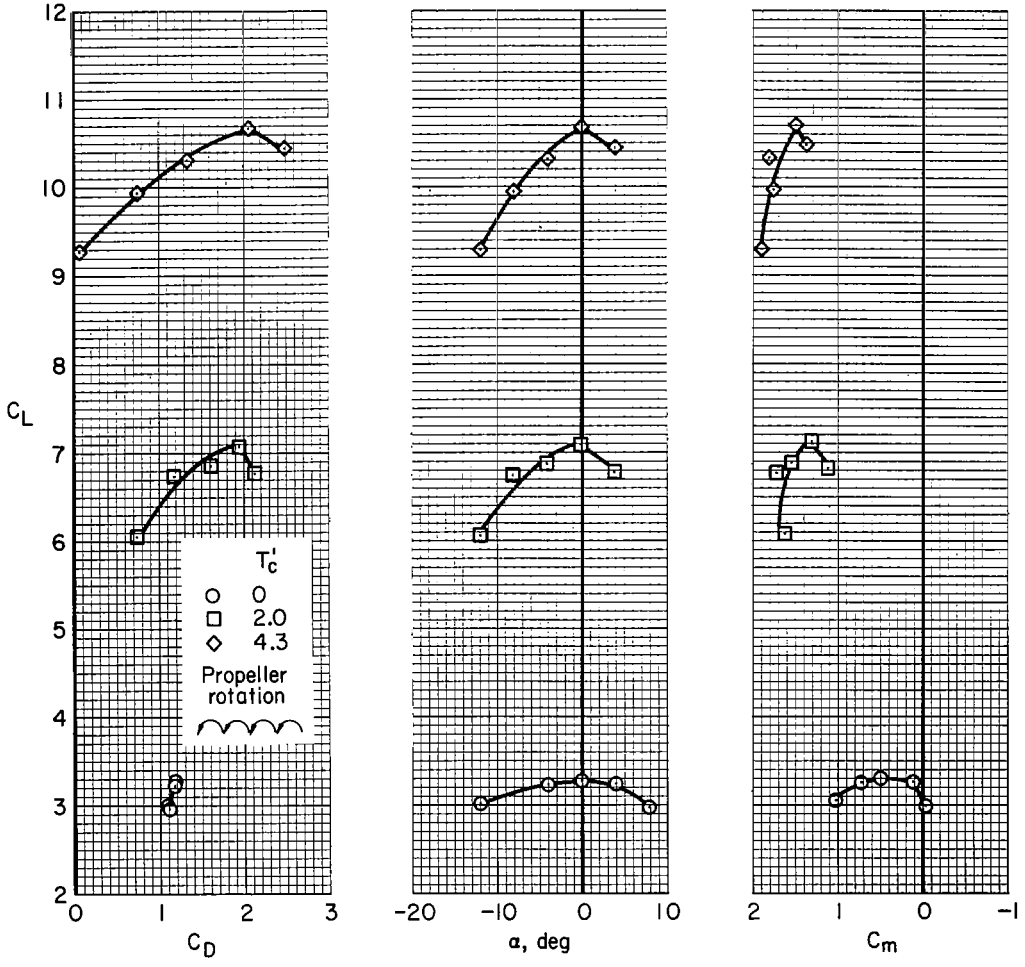

(d) $\frac{U}{V}$ = 6.6; tee tail.

Figure 20.- Continued.

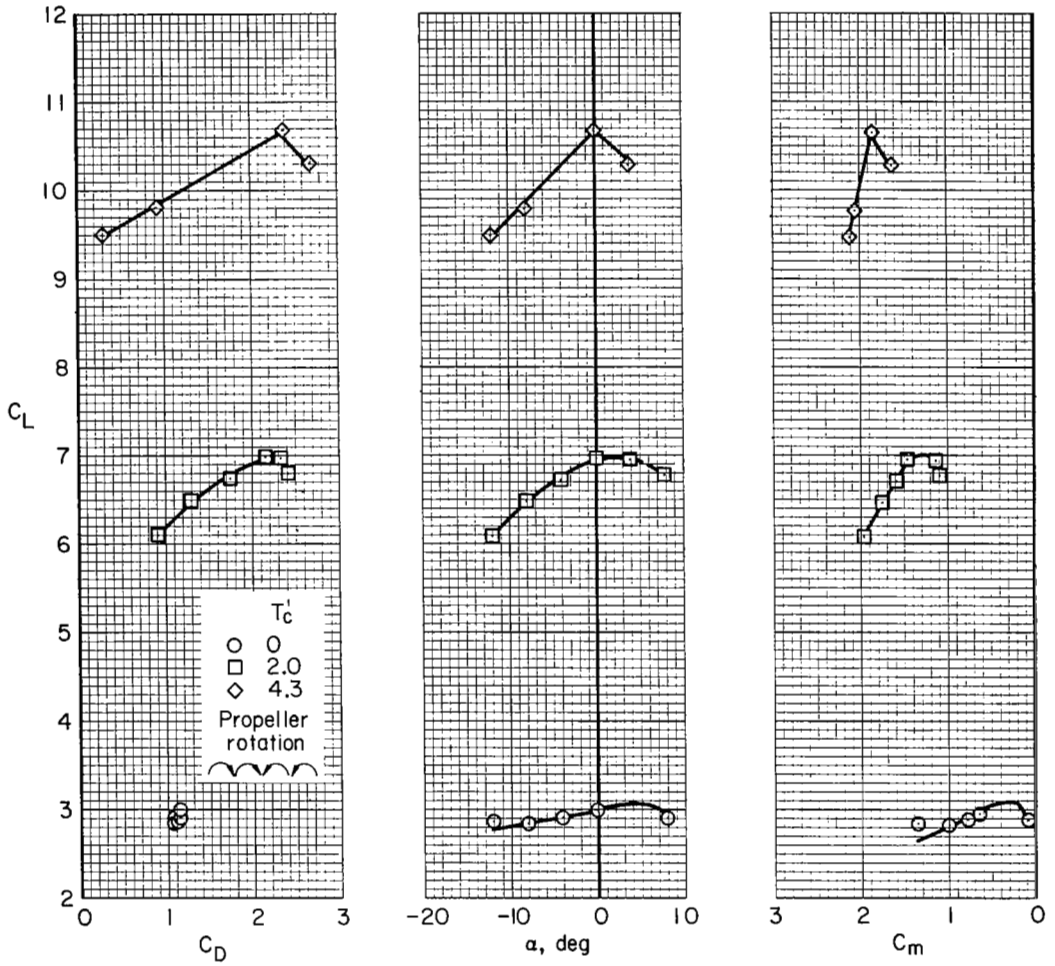

(e) $\frac{U}{V}$ = 6.6; tee tail.

Figure 20.- Continued.

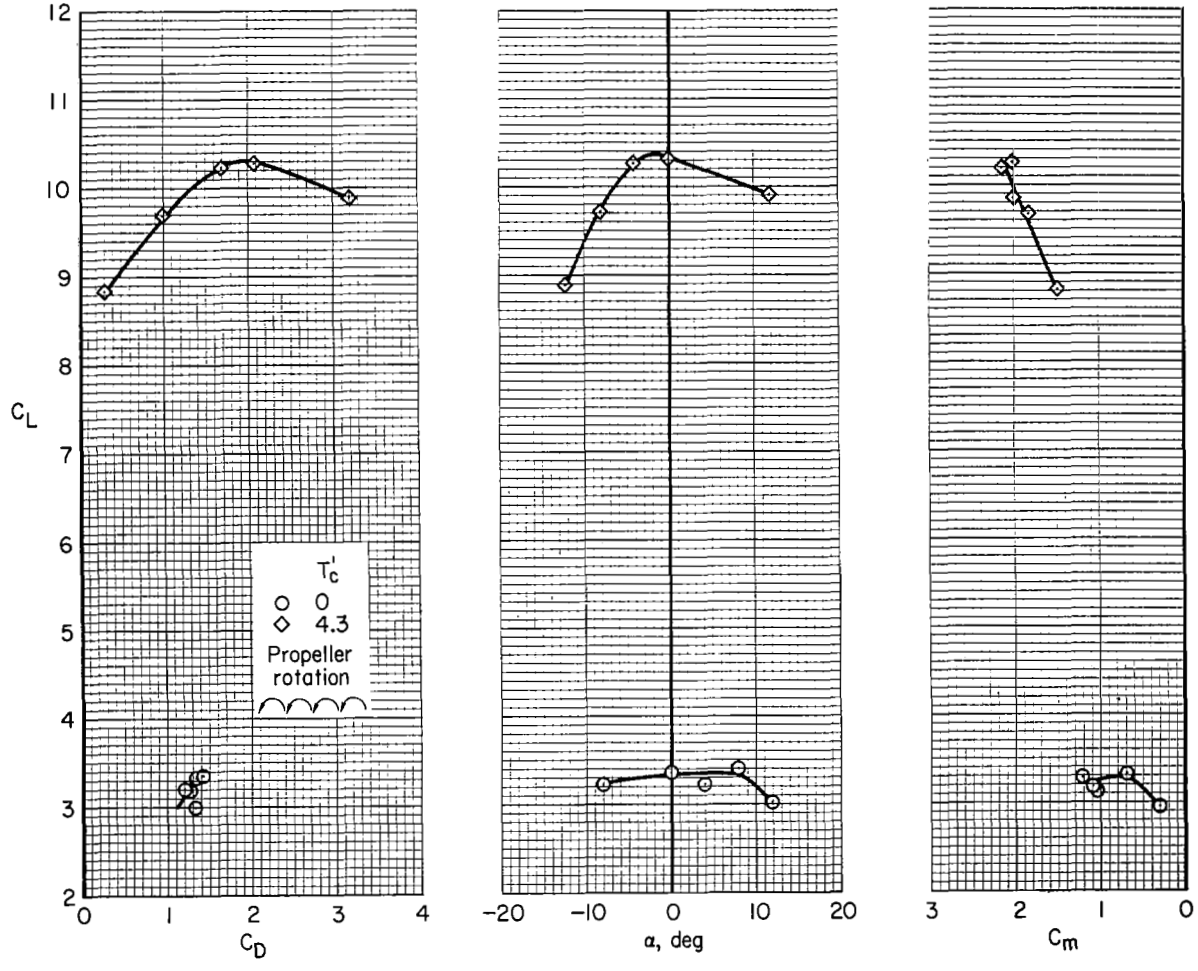

(f) $\frac{U}{V}$ = 6.6; low tail.

Figure 20.- Concluded.

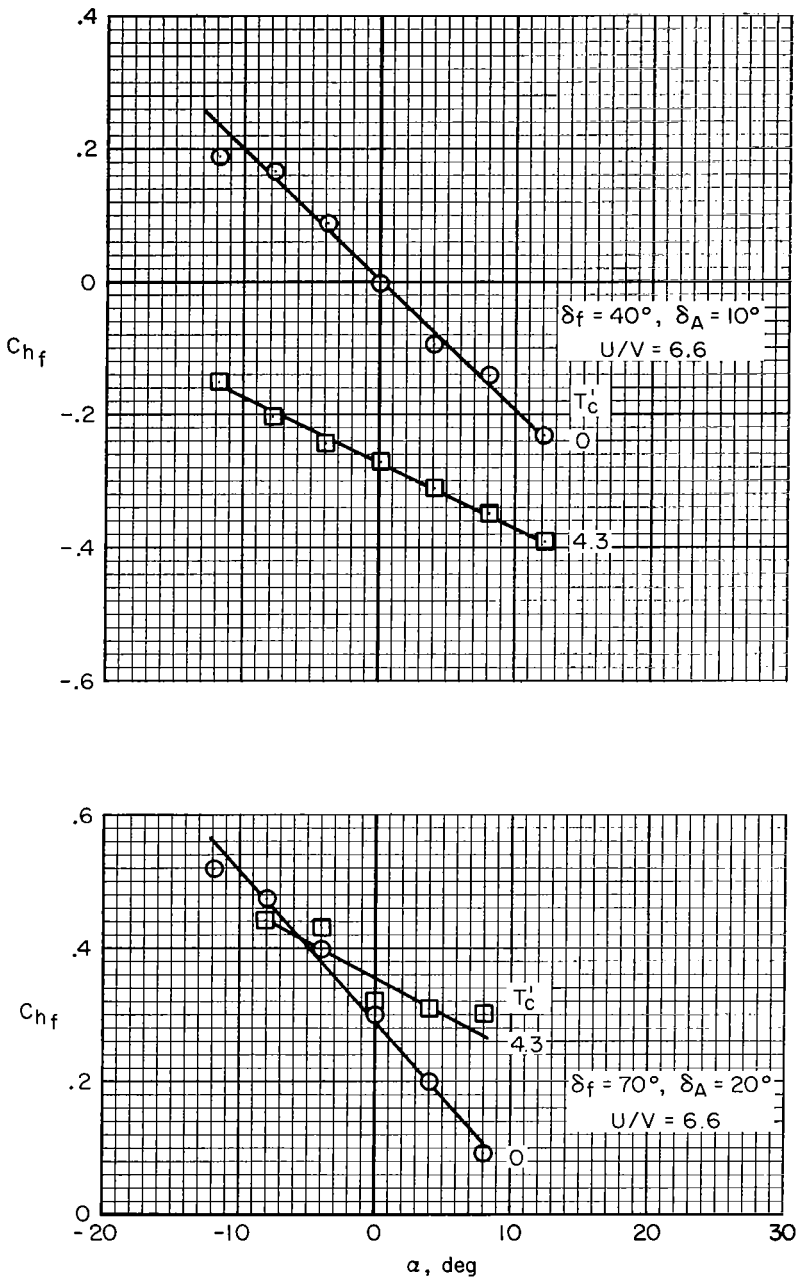

Figure 21.- Flap hinge moments.

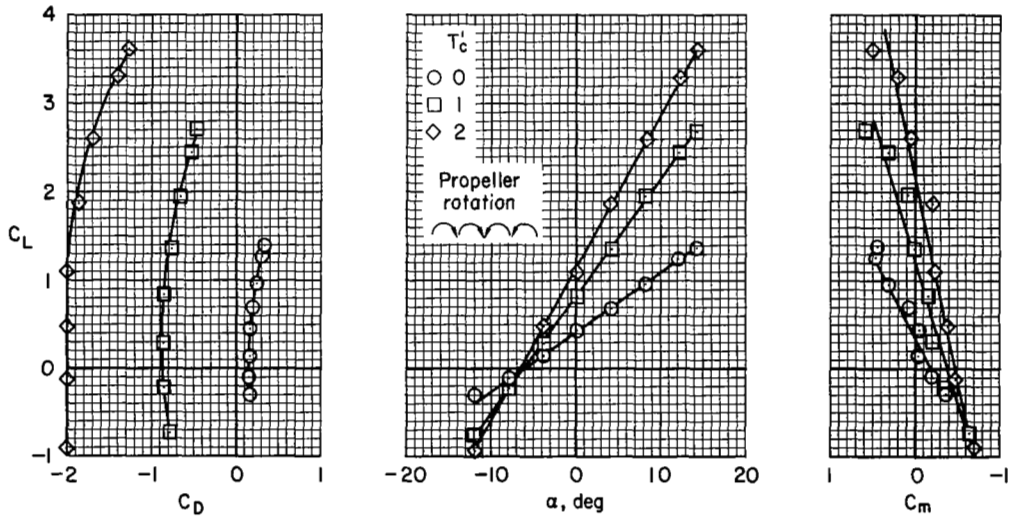

(a) $\delta_W = 0°$

Figure 22.- Aerodynamic characteristics; $\delta_f = 0°$, $\delta_A = 0°$, $\frac{U}{V} = 0$, tail off, nacelle spacing B.

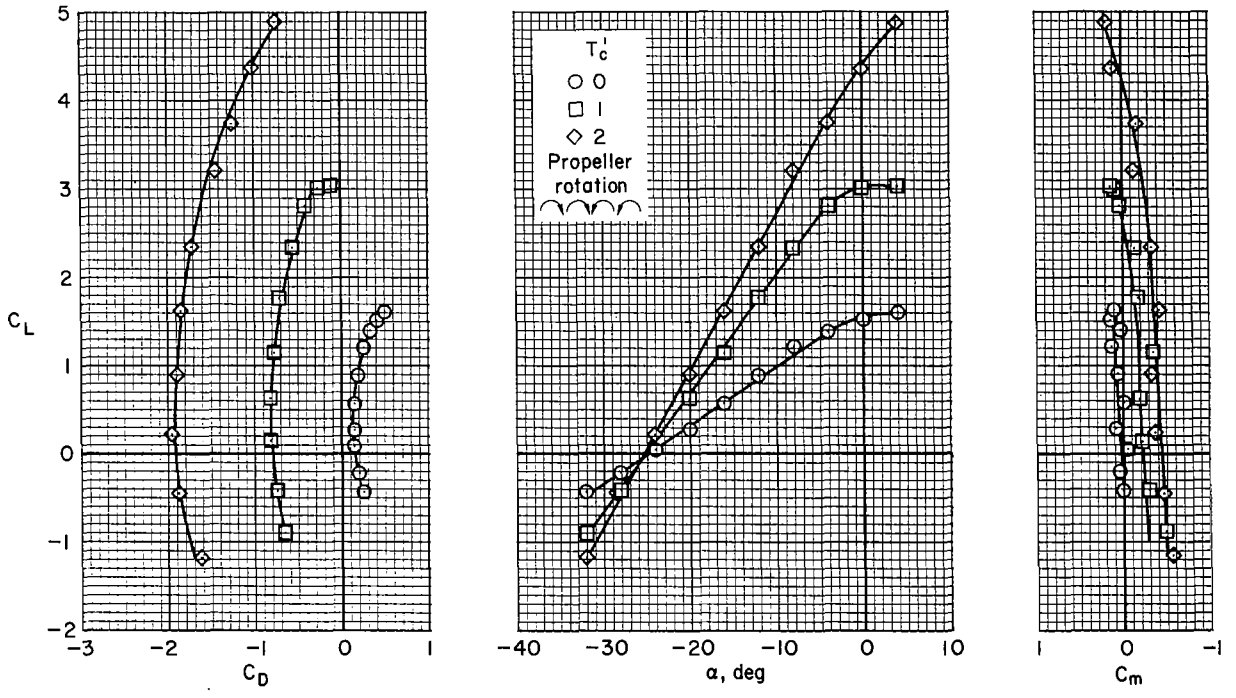

(b) $\delta_W = 20°$

Figure 22.- Concluded.

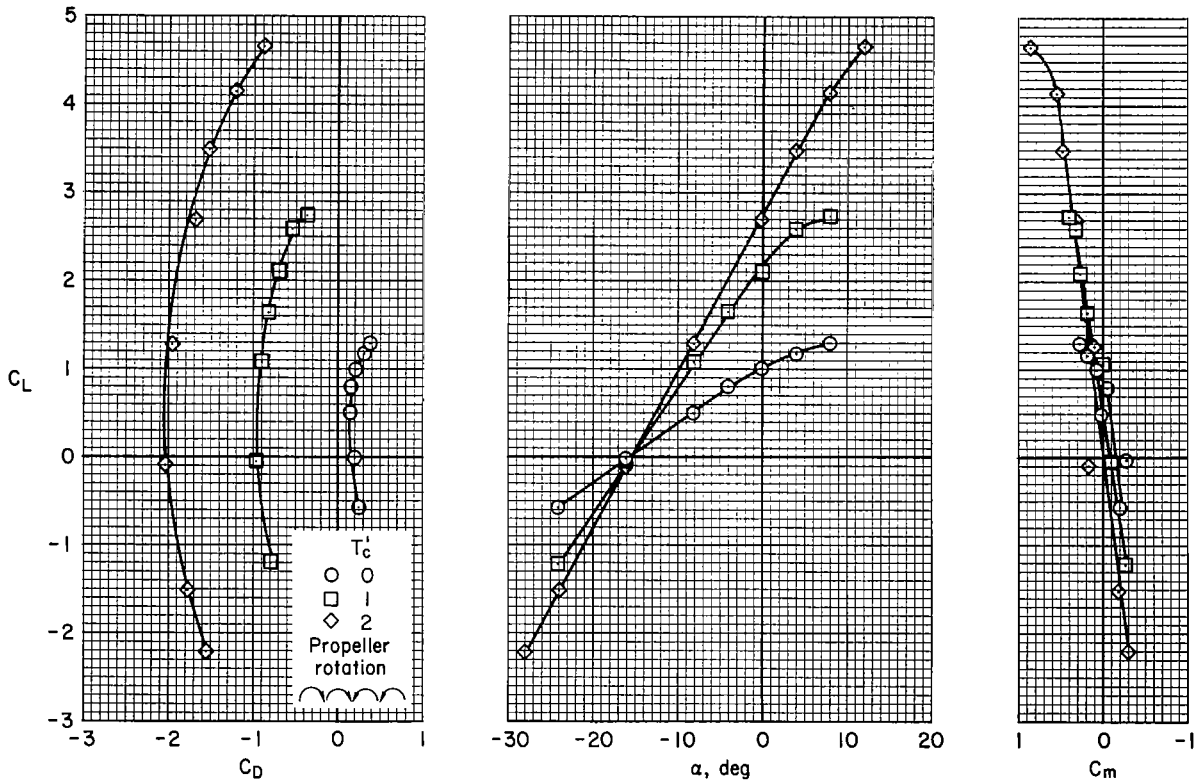

(a) $\delta_f = -10°$; $\delta_A = -10°$, $\frac{U}{V} = 0$, $\delta_W = 20°$

Figure 23.- Effect of negative flap deflection; tail off, nacelle spacing B.

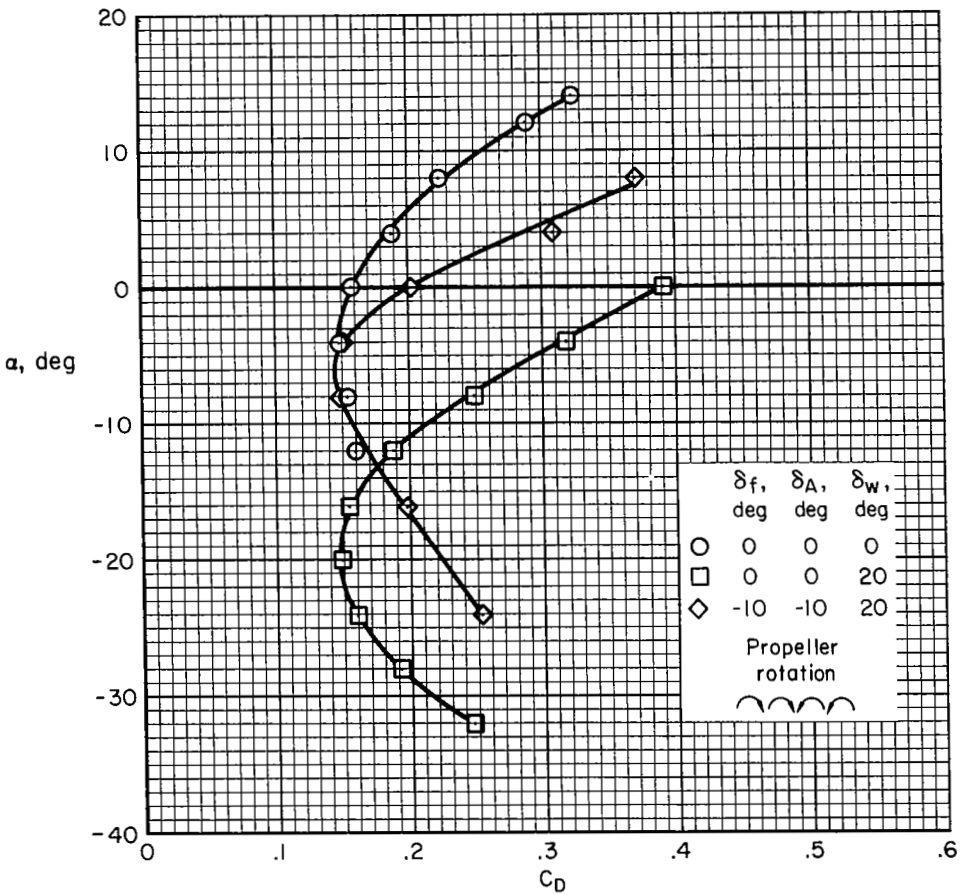

(b) C_D, α

Figure 23.- Concluded.

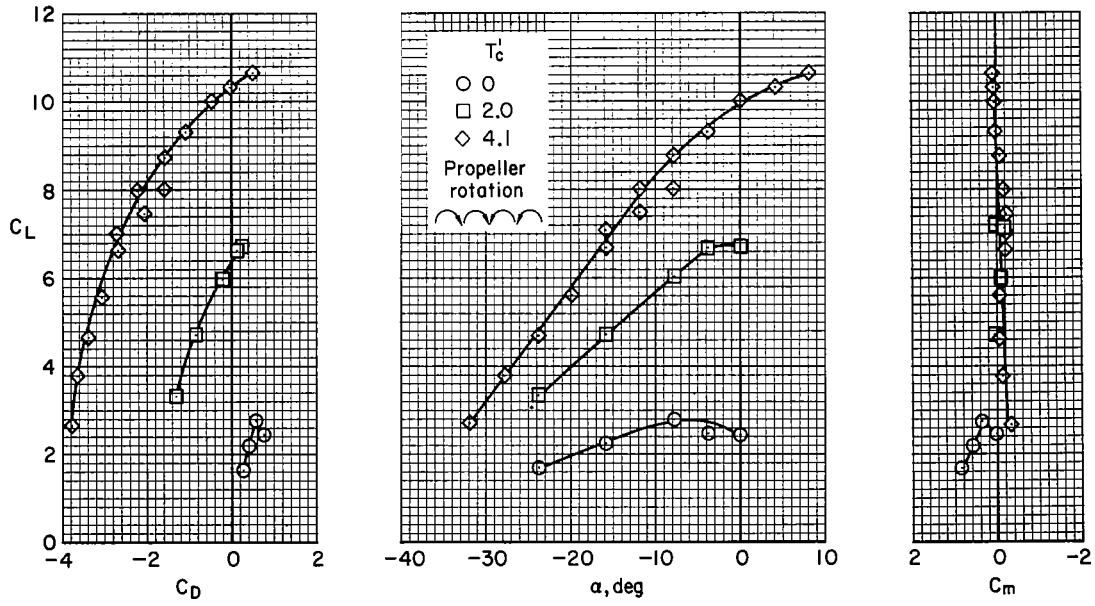

Figure 24.- Aerodynamic characteristics; $\delta_f = 25°$, $\delta_A = 10°$, $\frac{U}{V} = 4.0$, $\delta_W = 20°$, $\delta_T = -15°$, tail off, nacelle spacing B.

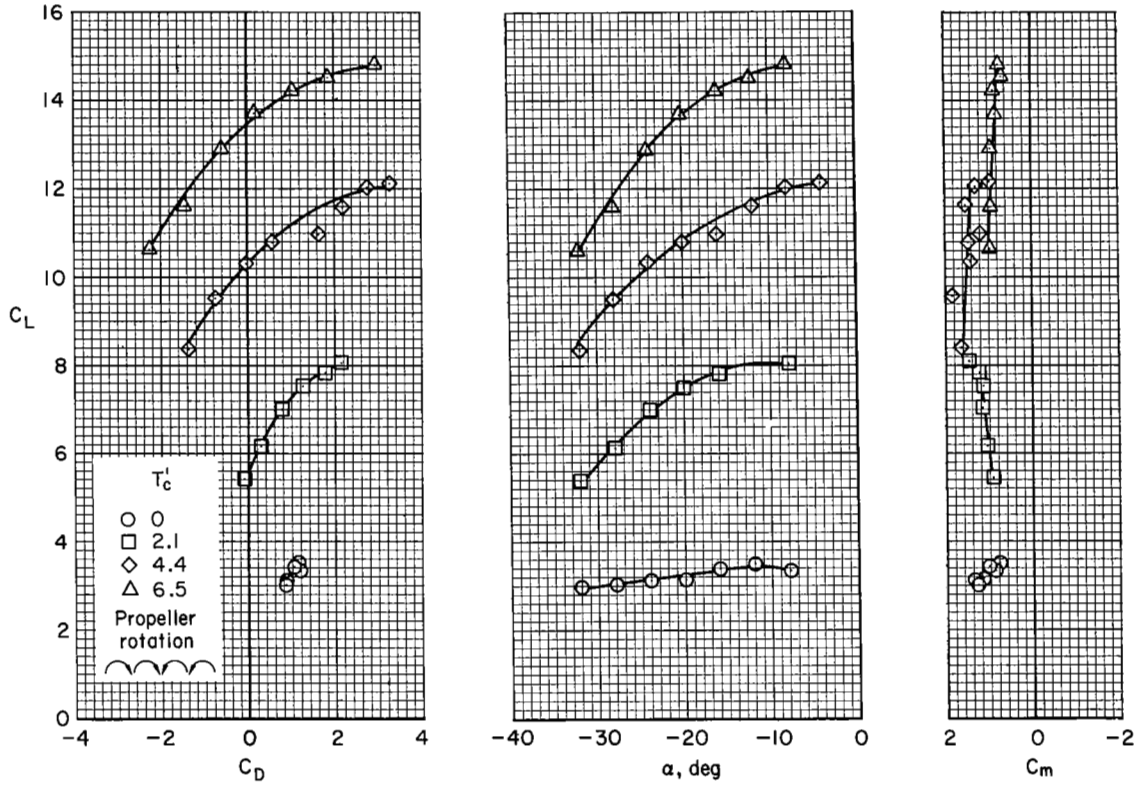

Figure 25.- Aerodynamic characteristics; $\delta_f = 55°$, $\delta_A = 20°$, $\frac{U}{V} = 6.6$, $\delta_W = 20°$, $\delta_T = -15°$, tail off, nacelle spacing B.

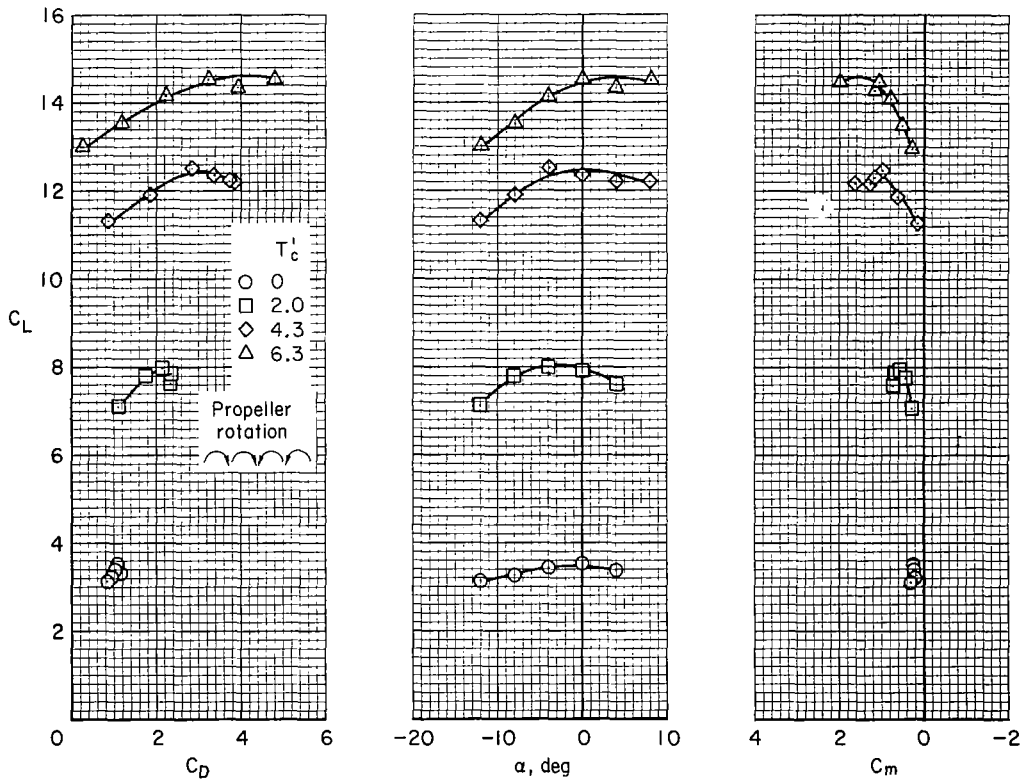

(a) $\delta_W = 0°$

Figure 26.- Aerodynamic characteristics; $\delta_f = 70°$, $\delta_A = 20°$, $\frac{U}{V} = 6.6$, tail off, nacelle spacing B.

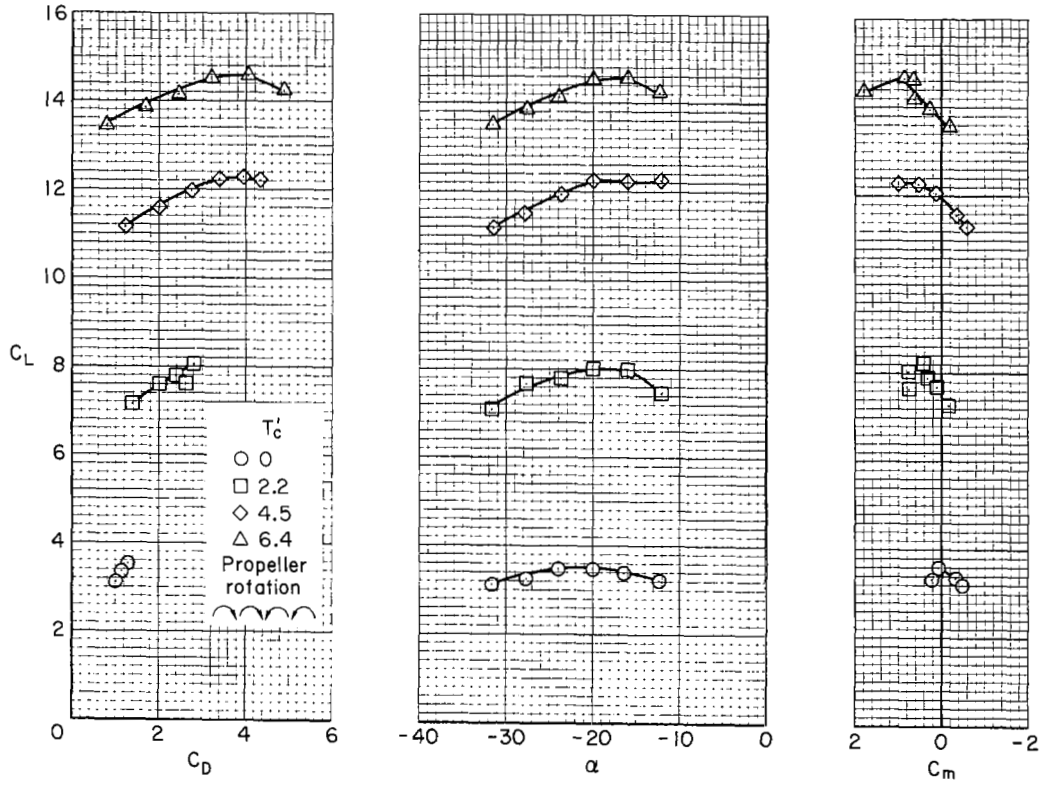

(b) $\delta_W = 20°$

Figure 26.- Concluded.

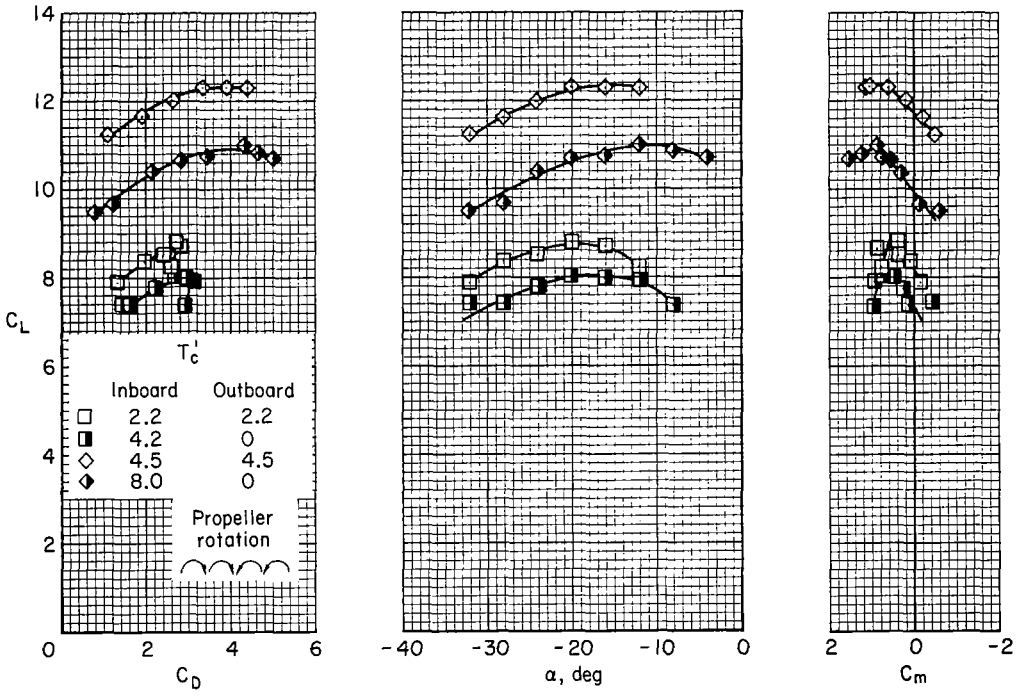

Figure 27.- Effect of differential propeller thrust; $\delta_f = 70°$, $\delta_A = 20°$, $\frac{U}{V} = 6.6$, tail off, $\delta_W = 20°$, nacelle spacing B.